A TNF-IL-1 circuit controls *Yersinia* within intestinal granulomas

Rina Matsuda[1,§], Daniel Sorobetea[1,§], Jenna Zhang[2,§], Stefan T. Peterson[1], James P. Grayczyk[1†], Beatrice Herrmann[1], Winslow Yost[1], Rosemary O'Neill[1], Andrea C. Bohrer[3], Matthew Lanza[1,‡], Charles-Antoine Assenmacher[1], Katrin D. Mayer-Barber[3], Sunny Shin[2,*], Igor E. Brodsky[1,*]

1. Department of Pathobiology, School of Veterinary Medicine, University of Pennsylvania, Philadelphia, PA 19104 USA
2. Department of Microbiology, Perelman School of Medicine, University of Pennsylvania, Philadelphia, PA 19104 USA
3. Inflammation and Innate Immunity Unit, Laboratory of Clinical Immunology and Microbiology, National Institute of Allergy and Infectious Diseases, National Institutes of Health, Bethesda, MD 20892, USA

[§]These authors contributed equally

[†]Current address: Oncology Discovery, AbbVie Inc., North Chicago, IL

[‡]Current address: Penn State Health Milton S Hershey Medical Center, Penn State College of Medicine, Hershey, PA 17033 USA

*correspondence: ibrodsky@vet.upenn.edu, ORCID 0000-0001-7970-872X

sunshin@pennmedicine.upenn.edu, ORCID 0000-0001-5214-9577

Summary

Monocytes restrict *Yersinia* infection within intestinal granulomas. Here, we report that monocyte-intrinsic TNF signaling drives production of IL-1 that signals to non-hematopoietic cells to control intestinal *Yersinia* infection within granulomas.

Abstract

Tumor necrosis factor (TNF) is a pleiotropic inflammatory cytokine that mediates antimicrobial defense and granuloma formation in response to infection by numerous pathogens. *Yersinia pseudotuberculosis* colonizes the intestinal mucosa and induces recruitment of neutrophils and inflammatory monocytes into organized immune structures termed pyogranulomas that control the bacterial infection. Inflammatory monocytes are essential for control and clearance of *Yersinia* within intestinal pyogranulomas, but how monocytes mediate *Yersinia* restriction is poorly understood. Here, we demonstrate that TNF signaling in monocytes is required for bacterial containment following enteric *Yersinia* infection. We further show that monocyte-intrinsic TNFR1 signaling drives production of monocyte-derived interleukin-1 (IL-1), which signals through IL-1 receptor on non-hematopoietic cells to enable pyogranuloma-mediated control of *Yersinia* infection. Altogether, our work reveals a monocyte-intrinsic TNF-IL-1 collaborative circuit as a crucial driver of intestinal granuloma function, and defines the cellular target of TNF signaling that restricts intestinal *Yersinia* infection.

Introduction

Granulomas form in response to a wide variety of infections, acting as barriers to pathogen dissemination[1,2]. Although generally considered protective, granulomas can also provide a replicative niche from which pathogens can spread, such as in immune-compromised patients that experience reactivation of latent *Mycobacterium tuberculosis*[3,4]. Moreover, pathogens within granulomas often persist in an antibiotic-resistant state and can pose a significant therapeutic challenge[5] Granulomas thus represent a localized niche within which pathogens persist and remain resistant to host immune clearance. Understanding how pathogens are controlled within granulomas remains an important question that could enable development of immunomodulatory treatments against infectious agents that persist within this niche.

Tumor necrosis factor (TNF) is a pleiotropic inflammatory cytokine associated with protection during granulomatous disease, notably tuberculosis[6–13]. While the role of TNF in maintaining intact granulomas is well-appreciated, its precise cellular targets and mechanisms of action remain elusive due to broad expression of its main receptor, TNFR1, and its pleiotropic downstream signaling functions, including induction of cell-extrinsic apoptosis, promoting cell survival, and mediating expression of pro-inflammatory gene programs[14–16]. TNF plays a critical role clinically in protection against infection by intracellular pathogens, as the extensive clinical use of anti-TNF blockade in the setting of auto-inflammatory disease is associated with increased risk of severe infection[16,17].

The enteropathogenic *Yersiniae*, which also include *Y. pseudotuberculosis* (*Yp*) and *Y. enterocolitica*, colonize the intestinal mucosa and lymphoid tissues of both mice and humans, triggering formation of pyogranulomas (PG) that are composed of

64 extracellular bacterial colonies in close association with neutrophils, bordered in turn by
65 monocytes and macrophages[18–25]. We recently demonstrated that PG containing viable
66 bacteria, inflammatory monocytes, and neutrophils form along the length of the
67 gastrointestinal tract early following oral *Yp* infection[25]. PG form in response to the activity
68 of Yersinia Outer Proteins (Yops), which are injected into host cells through the *Yersinia*
69 type III secretion system and block essential antimicrobial functions[25–27]. We further
70 demonstrated that inflammatory monocytes were critical for maintenance of PG
71 architecture and enabling neutrophils to overcome the activity of *Yp* virulence factors that
72 block host phagocytosis and oxidative burst[25]. However, the mechanisms by which
73 inflammatory monocytes mediate anti-*Yersinia* host defense are unclear.

74 Here, we demonstrate that monocytes serve as an essential cellular source of
75 TNF, which is required for host protection against *Yersinia*[28–30]. We find that signaling
76 through both TNF and IL-1 receptor are required to maintain PG control of *Yp.* Intriguingly,
77 monocyte-intrinsic TNF production and receptor signaling were required for PG
78 monocytes to produce IL-1, an inflammatory cytokine involved in control of other microbial
79 infections. IL-1 in turn signals to IL-1 receptor on non-hematopoietic cells to enable control
80 of intestinal *Yp* infection. Altogether, our study demonstrates that a monocyte-driven TNF-
81 IL-1 signaling circuit mediates the control of *Yp* infection within systemic and intestinal
82 sites and demonstrates that TNF and IL-1 collaborate via a feed-forward loop to promote
83 host defense against microbial infection.

Results

TNFR1 is required for organized pyogranuloma formation and restriction of Yersinia

We recently identified the formation of pyogranulomas (PG) in the murine intestinal mucosa during acute *Yersinia pseudotuberculosis (Yp)* infection, wherein inflammatory monocytes were required for neutrophil activation, maintenance of PG architecture, and bacterial clearance[25]. Nonetheless, the monocyte-derived signals required for the function and maintenance of these intestinal PG are unknown. Tumor necrosis factor (TNF) is critical for granuloma maintenance and bacterial control in the lung during tuberculosis infection[6–13], and we previously found that TNF signaling is necessary for the control of bacterial burdens following oral *Yersinia* infection[30]. Notably, while *Tnfr1*$^{-/-}$ mice formed similar numbers of macroscopic intestinal lesions as wild-type (WT) mice (Fig. S1A), histopathologic analyses revealed that intestinal lesions in *Tnfr1*$^{-/-}$ mice displayed a disorganized appearance and contained a central area of tissue necrosis that was strikingly similar to lesions that we recently described in monocyte-deficient mice[25], (Fig. 1A). In contrast to WT PG, which had robust immune cell aggregation and a small central *Yp* microcolony, *Tnfr1*$^{-/-}$ intestinal lesions contained limited immune cell infiltrate and an expanded *Yp* colony (Fig. 1A, B). In line with these histopathological findings, bacterial burdens in pyogranuloma-containing (PG+) intestinal punch biopsies and adjacent non-pyogranuloma (PG-) biopsies were elevated in *Tnfr1*$^{-/-}$ mice (Fig. 1C). Furthermore, *Tnfr1*$^{-/-}$ PG contained fewer monocytes, macrophages, and neutrophils, as determined by flow cytometry (Fig. 1D, S1B). Surface expression of the integrin CD11b, a marker of neutrophil activation[31–33], was significantly reduced in PG of *Tnfr1*$^{-/-}$ mice compared to WT controls (Fig. 1E), suggesting a defect in neutrophil activation in the absence of TNFR1

signaling, consistent with our recent findings of reduced neutrophil activation within PG in the absence of monocytes[25]. Additionally, *Tnfr1*$^{-/-}$ mice exhibited elevated bacterial burdens in the spleen and liver (Fig. 1F), consistent with our previous findings[30]. Notably, *Tnfr1*$^{-/-}$ mice succumbed to infection around day 8, while most WT mice survived (Fig. 1G). Overall, these data suggest that TNFR1 signaling is necessary to mediate functional intestinal PG formation and control of *Yp*.

TNFR1 signaling can enhance the ability of hematopoietic (immune) or non-hematopoietic (stromal) cells to control pathogens[10,11,13,30,34]. To test which compartment requires TNFR1 signaling to control *Yp*, we generated bone marrow chimeras in which TNFR1 expression was ablated on the immune or stromal compartment (Fig. S1C). Mice lacking TNFR1 in either the immune or stromal compartment had elevated bacterial burdens within PG compared to WT control chimeras, indicating that TNFR1 signaling is required non-redundantly in both hematopoietic and non-hematopoietic cells to mediate control of intestinal *Yp* (Fig. 1H). In contrast, mice lacking TNFR1 in immune cells had elevated bacterial burdens in the systemic tissues, while mice lacking TNFR1 in stromal cells had similar bacterial burdens in systemic tissues as WT controls (Fig. 1I). Taken together, these results demonstrate that TNFR1 signaling in both hematopoietic and non-hematopoietic cells contribute to bacterial control in the intestine, while TNFR1 signaling specifically in immune cells is required for bacterial control in the systemic tissues during acute *Yp* infection.

Autocrine TNF signaling in monocytes is required for control of Yersinia

TNF receptor expression is widespread on hematopoietic cells, raising the question of which specific cells are the necessary targets of TNF signaling for control of *Yp* infection. We previously demonstrated that CCR2-deficient mice lacking circulating monocytes fail to form functional intestinal PG, are unable to control *Yp* burdens, and succumb to infection[25]. Given the similar outcomes of infection and histopathological appearance of PG in TNFR1- and CCR2-deficient mice, we sought to test the hypothesis that TNF is either produced or detected by monocytes. To do this, we generated mice in which TNFR1 was specifically deleted on inflammatory monocytes by means of mixed BM chimeras where irradiated wild-type recipient mice were reconstituted with a 1:1 ratio of $Ccr2^{gfp/gfp}$:$Tnfr1^{-/-}$ or $Ccr2^{gfp/gfp}$:*WT* control BM cells (Fig. 2A). Because circulating monocytes in these chimeric mice are derived from the $Tnfr1^{-/-}$ or WT BM cells, respectively, this approach generates mice in which circulating $CCR2^{+}$ monocytes lacked or expressed TNFR1, respectively, with other hematopoietic cell types being comprised of a 1:1 mixture of these genotypes (Fig. S2A). Intriguingly, mice lacking TNFR1 specifically on $CCR2^{+}$ monocytes formed lesions with expanded bacterial colonies and failed to control *Yp* infection, largely recapitulating the phenotype of mice lacking CCR2 in the hematopoietic system altogether (Fig. 2B-D). Importantly, this defect in bacterial control was not due to a lack of TNFR1 expression on 50% of other immune cells, as mixed chimeras from $Tnfr1^{-/-}$:*WT* mice still had significantly lower bacterial burdens relative to $Tnfr1^{-/-}$:$Ccr2^{gfp/gfp}$ mice, notably in systemic tissues (Fig. S2B, C). Mice lacking TNFR1 expression on all hematopoietic cells had significantly higher burdens than mice lacking TNFR1 on monocytes alone (Fig. S2B). Altogether, these data suggest that

TNFR1 signaling in monocytes is essential for their protective role against *Yp* infection, and that TNFR1 has additional important roles in other cell types beyond monocytes.

Multiple immune cell types produce TNF in response to inflammatory signals, including monocytes, which we previously observed to be a major source of TNF during *Yp* infection[35]. Thus, we considered that monocytes might be an important source as well as recipient of the TNF signal to enable control of *Yp* infection. We therefore reconstituted irradiated wild-type recipient mice with a 1:1 ratio of *Ccr2*$^{gfp/gfp}$:*Tnf*$^{-/-}$ or *Tnf*$^{-/-}$:*WT* control BM cells, in order to generate cohorts of mice in which circulating CCR2^{+} monocytes lacked or retained the ability to produce TNF, respectively, with other hematopoietic cell types being comprised of a 1:1 mixture. Strikingly, mice lacking TNF specifically in monocytes failed to control *Yp* infection in the spleen and liver, with equal burdens to those completely lacking TNF production in all hematopoietic cells (Fig. 2E, F). Altogether, our findings demonstrate that autocrine TNF signaling in monocytes is required to control enteric *Yp* infection.

TNFR1 signaling in monocytes controls Yp infection independently of RIPK1 kinase-induced cell death

TNFR1 can mediate inflammatory gene expression or promote cell-extrinsic apoptosis in response to infection by pathogens, including *Yersinia*[36–41]. *Yp*-induced cell death is triggered by YopJ-induced blockade of IKK signaling and involves contributions from both TLR4/TRIF and TNFR1 signaling through the adapter kinase RIPK1[35,42–47]. We previously demonstrated that mice specifically lacking RIPK1 kinase activity (*Ripk1*^{K45A}) in hematopoietic cells fail to form intact MLN PG and rapidly succumb to *Yp* infection[35].

Furthermore, activation of gasdermin D and gasdermin E in macrophages and neutrophils, respectively, downstream of RIPK1 kinase activity promotes control of *Yp* infection[48]. *Ripk1*^{K45A} mice formed necrotic intestinal lesions and were deficient in restricting *Yp* burdens, consistent with prior findings (Fig. 3A-C). These data provoked the hypothesis that monocyte-intrinsic TNFR1 signaling promotes anti-*Yersinia* host defense through activation of RIPK1-induced monocyte cell death. To directly test this, we generated mixed BM chimeras in which irradiated WT recipient mice were reconstituted with a 1:1 ratio of *Ccr2*$^{gfp/gfp}$:*Ripk1*^{K45A} or *Ccr2*$^{gfp/gfp}$:*WT* control BM cells. Following reconstitution, mice contained circulating CCR2^{+} monocytes that either lacked or expressed RIPK1 kinase activity, respectively, with all other hematopoietic cells being equally reconstituted by both donor bone marrow progenitors (Fig. S3A). Surprisingly, in contrast to hematopoietic loss of RIPK1 kinase activity, monocyte-specific ablation of RIPK1 kinase activity had no effect on the ability of mice to form intact intestinal PG or control enteric *Yp* infection (Fig. 3D-F), indicating that RIPK1 kinase activity is dispensable in monocytes to control *Yp* infection downstream of TNF signaling. Our previous findings demonstrated that the acute susceptibility of *Ripk1*^{K45A} mice is reversed in the setting of infection with YopJ-deficient bacteria, illustrating that RIPK1 kinase-induced cell death is necessary to counteract the blockade of immune signaling by YopJ[35]. However, *Tnfr1*$^{-/-}$ mice still formed necrotic intestinal PG, were unable to control bacterial burdens in systemic tissues, and succumbed to infection by YopJ-deficient bacteria (Fig. 3G-I). Collectively, these data indicate TNFR1 signaling contributes to anti-*Yersinia* host defense via a mechanism distinct from RIPK1-induced cell death. We recently reported that intestinal PG form in response to the activities of the actin

cytoskeleton-disrupting effectors YopE and YopH, and that monocytes counteract YopH-mediated blockade of innate immunity[25]. YopE and YopH both block phagocytosis and the oxidative burst through disruption of actin cytoskeleton rearrangement[49–58]. However, whether TNFR1 is required to overcome the immune blockade posed by YopE and YopH is unknown. Strikingly, TNFR1-deficient mice survived infection with *yopEH* mutant *Yp* (Fig. 3J), indicating that TNFR1 signaling counteracts the activity of YopE and YopH. However, in contrast to our previous findings with CCR2-deficient mice[25], *Tnfr1*$^{-/-}$ mice were not able to control either single *Yp* mutant, although there was a significant delay in mortality in response to infection with *yopH* mutant bacteria (Fig. S3B). Together, these findings demonstrate that TNFR1-mediated restriction of enteric *Yp* infection is independent of RIPK1-induced cell death, and instead counteracts the anti-phagocytic and reactive oxygen-blocking activities of YopE and YopH.

Cell-intrinsic TNFR1 signaling is required for maximal IL-1 production within intestinal pyogranulomas during Yersinia infection

Our findings indicate that while TNFR1 expression on monocytes is critical for effective intestinal PG formation and control of *Yp* infection, monocyte-intrinsic RIPK1 kinase activity is dispensable for PG formation and bacterial restriction. This suggests that RIPK1 kinase-independent mechanisms mediate monocyte-dependent control of *Yp* downstream of TNFR1 signaling. We therefore hypothesized that TNFR1 signaling in monocytes may contribute to control of *Yp* infection via promoting inflammatory cytokine production. Multiplex cytokine profiling of intestinal PG from mixed BM chimeric mice lacking monocyte-intrinsic TNFR1 expression revealed that IL-1α levels were significantly

decreased, in contrast to other pro-inflammatory cytokines such as IL-6 and KC (Fig. 4A, S4A). Neither IL-1α nor IL-1β were detected in the sera of these mice, suggesting that IL-1 production in response to TNFR1 signaling is localized to intestinal tissues during *Yp* infection (Fig. S4B).

Since TNFR1 expression on monocytes is required for intestinal PG formation and restriction of bacterial burdens, we hypothesized that TNFR1 signaling promotes IL-1 production by monocytes within intestinal PG. Indeed, intracellular cytokine staining demonstrated that both IL-1α and IL-1β expression were decreased in both monocytes and neutrophils in *Tnfr1*$^{-/-}$ PG, indicating that TNFR1 signaling is necessary for maximal IL-1 production in both monocytes and neutrophils within intestinal PG (Fig. 4B). We next asked whether TNFR1 signaling functions in a cell-intrinsic or -extrinsic manner to promote IL-1 cytokine production. To distinguish between these possibilities, we generated mixed bone marrow chimeras in which lethally irradiated WT recipients were reconstituted with a 1:1 mixture of WT and *Tnfr1*$^{-/-}$ bone marrow or entirely reconstituted with *Tnfr1*$^{-/-}$ bone marrow as a positive control. Importantly, there was no competitive defect in reconstitution by *Tnfr1*$^{-/-}$ cells in the mixed chimera setting, as these mice contained 1:1 ratio of WT and *Tnfr1*$^{-/-}$ immune cells within the PG and spleen (Fig. S4C**)**. Strikingly, IL-1 production was reduced in both monocytes and neutrophils lacking TNFR1 relative to WT cells isolated from the same mice, demonstrating that cell-intrinsic TNFR1 is required for optimal production of IL-1 in monocytes and neutrophils (Fig. 4C, D, S4D). To ask if TNF signals in an autocrine fashion to upregulate its own expression, we measured intracellular TNF in these WT:*Tnfr1*$^{-/-}$ mixed chimeras. TNF levels were reduced in both monocytes and neutrophils lacking TNFR1 relative to WT cells isolated

from the same intestinal PG, demonstrating that TNFR1 signals in a feedforward loop to promote TNF production in a cell-intrinsic fashion (Fig. S4E). Overall, these data show that cell-intrinsic TNFR1 signaling is necessary for maximal IL-1 production in myeloid cells within intestinal PG, raising the question of whether IL-1 production downstream of TNFR1 signaling in monocytes contributes to control of *Yp* during early intestinal infection.

IL-1 is required for organized pyogranuloma formation and intestinal control of Yersinia

IL-1 plays a critical role in host defense by promoting immune cell recruitment and activation, cytokine production, angiogenesis, and vascular permeability[59–64]. Mice lacking IL-1 signaling are more susceptible to systemic *Yersinia* infection[48,65,66]. However, the role of IL-1 signaling during enteric *Yp* infection and downstream of TNF receptor signaling is unclear. IL-1β production has been proposed to promote increased intestinal permeability and barrier dysfunction[67], suggesting multifaceted roles for IL-1 signaling within specific compartments and stages of infection. We considered the possibility that TNFR1-mediated restriction of enteric *Yp* infection and intestinal PG formation occurs in part via induction of IL-1 production from monocytes. To test the contribution of IL-1 signaling in control of enteric *Yp* infection, we infected *Il1r1*$^{-/-}$ mice, which lack IL-1R and cannot respond to IL-1 cytokines. *Il1r1*$^{-/-}$ mice had significantly higher bacterial burdens than WT mice in the intestine, specifically in Peyer's Patches, PG+, and PG- tissue (Fig. 5A). Notably, the intestinal lesions in *Il1r1*$^{-/-}$ mice showed extensive loss of organization and contained a central area of tissue necrosis as compared to those found in WT mice (Fig. 5B). Strikingly, the intestinal lesions in *Il1r1*$^{-/-}$ mice bore substantial resemblance to the intestinal lesions seen in *Ccr2*$^{gfp/gfp}$ mice[25] and *Tnfr1*$^{-/-}$ mice (Fig. 5B and 1A). *Il1r1*$^{-/-}$

mice also succumbed to infection to a greater extent than WT mice (Fig. 5C). However, at day 5 post-infection, bacterial burdens in systemic organs were broadly comparable to those of WT mice (Fig. S5A). Collectively, these results suggest that consistent with PG-specific TNF-dependent IL-1 production, IL-1-mediated *Yp* restriction occurs in the intestine during early infection and that there are likely other non-IL-1-mediated mechanisms induced downstream of TNF signaling that contribute to systemic control.

IL-1R initiates intracellular signaling cascades in response to both IL-1α and IL-1β. To test whether IL-1α and IL-1β are individually important for intestinal PG formation and *Yp* control, we infected *Il1a*$^{-/-}$ and *Il1b*$^{-/-}$ mice. Compared to WT mice, both *Il1a*$^{-/-}$ and *Il1b*$^{-/-}$ mice had elevated bacterial burdens in PP and PG+, but not in PG- tissue (Fig. 5D), in contrast to *Il1r1*$^{-/-}$ mice which had elevated bacterial burdens in all three intestinal compartments. Like *Il1r1*$^{-/-}$ mice, *Il1a*$^{-/-}$ and *Il1b*$^{-/-}$ mice overall had similar bacterial burdens in systemic organs as WT mice on day 5 post-infection (Fig. S5A). Collectively, these results suggest that IL-1α and IL-1β may have overlapping roles in restricting early enteric *Yp* infection, and in the absence of one, the other may compensate. Intriguingly, *Il1a*$^{-/-}$ mice had a comparable survival defect to *Il1r1*$^{-/-}$ mice, whereas *Il1b*$^{-/-}$ mice were similar to WT mice in survival following *Yp* infection (Fig. 5E). Collectively, these results indicate that IL-1R signaling is important for intestinal PG formation and control of enteric *Yp* infection, and may constitute a mechanism by which TNFR1 signaling controls local intestinal infection.

Monocyte-derived IL-1 signals to non-hematopoietic cells to restrict Yersinia in intestinal pyogranulomas

289 Our findings demonstrate that with PG, autocrine TNF signaling in inflammatory
290 monocytes promotes cell-intrinsic IL-1 production and subsequent IL-1R signaling
291 promotes anti-*Yp* immune defense. However, whether monocyte-derived IL-1 is
292 specifically required for control of intestinal *Yp* has not been tested. We therefore infected
293 mixed BM chimeras in which irradiated wild-type recipient mice were reconstituted with a
294 1:1 ratio of *Il1ab*$^{-/-}$:*Ccr2*$^{gfp/gfp}$ bone marrow cells to generate cohorts of mice specifically
295 lacking IL-1α and IL-1β production in monocytes, along with mice reconstituted with *Il1ab*$^{-}$
296 $^{/-}$:WT bone marrow or 100% *Il1ab*$^{-/-}$ bone marrow (Fig. S6A). Critically, mice specifically
297 lacking IL-1α and IL-1β in monocytes had significantly elevated bacterial burdens in PG,
298 recapitulating elevated bacteria burdens in PG of hematopoietic-deficient IL-1α and IL-1β
299 chimeric mice and indicating that monocyte-derived IL-1 is important for restricting
300 infection within intestinal PG (Fig. 6A). Bacterial burdens in PG- punch biopsies and
301 systemic organs were broadly similar across chimeric mice genotypes (Fig. 6A, S6B),
302 suggesting that IL-1 production from other cell types besides monocytes may contribute
303 to intestinal infection restriction. Collectively, these data suggest that multiple cellular
304 sources of IL-1 drive restriction of *Yp*. In agreement with our previous finding that TNFR1-
305 deficient mice have a defect in IL-1 production within PG, monocyte-derived IL-1 was
306 critical for control of bacterial burdens within PG, indicating that IL-1 production from
307 monocytes plays a significant role in TNF-dependent control within this intestinal niche.
308 Multiple cell types express *Il1r1* and respond to IL-1 signaling. In other infectious
309 settings, IL-1R signaling specifically in the stromal compartment is critical for antibacterial
310 defense[62,64,68–71]. We therefore considered that IL-1R signaling in stromal cells may be
311 critical for formation and maintenance of intestinal PG as well as *Yp* restriction. To test

this, we generated BM chimeric mice in which irradiated *Il1r1*$^{-/-}$ mice were reconstituted with WT BM. Additionally, irradiated WT mice were reconstituted with either *Il1r1*$^{-/-}$ bone marrow or a 1:1 ratio of *Il1r1*$^{-/-}$:WT bone marrow. Notably, mice lacking IL-1R in the stromal compartment had elevated bacterial burdens in both intestinal (PP, PG+ and PG) and systemic (liver and spleen) tissues following oral *Yp* infection compared to WT control chimeras, while mice lacking IL-1R in the hematopoietic compartment had similar bacterial burdens to WT control chimeras (Fig. 6B, C). Overall, our findings demonstrate that IL-1R signaling on the stromal compartment is required to restrict *Yp* infection both in the intestinal and systemic tissues.

Discussion

Granulomas are organized biological structures containing multiple immune cell types working in concert with stromal cells to sequester pathogens that are difficult to clear[1,2]. *Yersinia pseudotuberculosis* induces the formation of granulomatous lesions in both the human and murine intestine[18–25]. Here, we uncover a TNF/IL-1 signaling circuit that promotes restriction of enteropathogenic *Yp* within intestinal pyogranulomas. Notably, we find that autocrine TNF signaling on inflammatory monocytes was necessary to promote cell-intrinsic IL-1 production, which signaled on the non-hematopoietic compartment to elicit control of *Yp* within intestinal pyogranulomas.

TNF has a well-established role in granuloma formation and maintenance[6–13]. Anti-TNF therapy triggers reactivation of dormant *Mycobacterium tuberculosis* infection[8,72,73], and TNF promotes macrophage-dependent control of *Salmonella* replication within granulomas during chronic *Salmonella* infection[34]. TNF promotes multiple antimicrobial activities of macrophages that are critical for granuloma formation and control of tuberculosis[10,11,13,74]. However, excessive TNF causes macrophage cell death that can be detrimental to bacterial control[75]. Some pathogens counteract the pro-inflammatory effects of TNF signaling within granulomas. *Salmonella* injects the T3SS effector SteE to induce anti-inflammatory M2 macrophage polarization, countering TNF-driven M1 polarization to hinder bacterial clearance[34]. In line with our previous observations that TNFR1 is required for protection against *Yp*[30], our findings highlight a key role for TNF signaling in promoting intestinal pyogranuloma formation and function during enteropathogenic *Yp* infection.

343 TNFR1 signaling promotes *Yp*-induced cell death via RIPK1 activity, and we
344 previously found that RIPK1 activity was necessary for control of *Yp* infection[35]. However,
345 while deficiency in RIPK1 kinase activity led to disrupted intestinal PG formation during
346 early infection, we surprisingly found that RIPK1 kinase activity was dispensable in
347 monocyte-lineage cells for PG formation and bacterial restriction. These findings suggest
348 that two distinct pathways are necessary for protection against enteric *Yersinia* infection:
349 1) a monocyte-intrinsic TNFR1 pathway that amplifies inflammatory cytokine production
350 in monocytes, and 2) a YopJ-induced RIPK1 kinase-mediated cell death of non-monocyte
351 cells. Notably, neutrophils undergo GSDME-dependent pyroptosis downstream of RIPK1
352 kinase activity, which contributes to restriction of *Yp* infection *in vivo*[48]. Future studies will
353 elucidate whether RIPK1 kinase-dependent neutrophil cell death promotes control of *Yp*.
354 We found that TNFR1 signaling on PG monocytes enhanced cell-intrinsic IL-1
355 production, consistent with our previous findings that monocyte-deficient intestinal PG
356 have reduced IL-1 levels[25]. While TNF receptor signaling amplifies inflammasome
357 activation, an important step in IL-1 processing[76–78] very few studies have described
358 TNFR-signaling-mediated IL-1 production specifically. In the context of *Legionella*
359 *pneumophila* infection, IL-1 signaling induces TNF production in uninjected bystander
360 cells in order to overcome virulence-induced host protein blockade that prevents TNF
361 production from infected cells[61,62] Interestingly, *Yersinia* YopJ suppresses inflammatory
362 cytokine expression including TNF expression[43] Whether uninjected bystander
363 monocytes are the critical source of TNF during enteric *Yp* infection remains unexplored.
364 TNF has been shown to induce macrophage polarization and promotion of IL-1β

365 expression via sterol response element binding factors[16] How TNF receptor signaling
366 augments IL-1 production during *Yp* infection is still unknown.

367 IL-1R signaling is critical for infection control during tuberculosis infection and loss
368 of IL-1R signaling leads to expansion of pathologic lesions in the lung[79–84]. We observed
369 that in the absence of IL-1R, mice failed to form organized intestinal pyogranulomas and
370 had elevated intestinal *Yp* burdens, corroborating previous reports that IL-1R signaling
371 promotes anti-*Yersinia* defense[48,65,66]. Intriguingly, systemic bacterial burdens were
372 similar between WT mice and mice lacking IL-1R signaling, suggesting that there TNF
373 signaling induces other mechanisms of bacterial restriction beyond IL-1-mediated
374 protection. Mice lacking IL-1R signaling were more susceptible than mice lacking IL-1α
375 or IL-1β alone, indicating that both cytokines contribute non-redundantly to bacterial
376 restriction. While mice deficient in IL-1α exhibited elevated mortality, there was no
377 difference in mortality in mice deficient in IL-1β. Perhaps during the early intestinal stage
378 of infection, IL-1α and IL-1β mediate overlapping mechanisms of *Yersinia* restriction,
379 while at later stages of infection, IL-1α is largely responsible for IL-1R-mediated control.
380 IL-1α is a critical mediator of intestinal inflammation and inflammatory cell recruitment
381 during *Yersinia enterocolitica* infection[85]. In contrast, IL-1β contributes to *Yersinia*
382 restriction[48] but also promotes intestinal barrier permeability and translocation of
383 commensal bacteria downstream of YopJ activity[86]. Together, these observations
384 suggest that tight regulation of intestinal IL-1 signaling is important to combat *Yersinia*
385 infection while avoiding excessive tissue damage and loss of intestinal barrier function.

386 While IL-1β is released from hematopoietic cells downstream of inflammasome
387 activation, IL-1α is more broadly expressed across cell types and can function in multiple

388 locations, including within the nucleus, as a membrane-bound cytokine, or as an alarmin
389 released from dying cells[87]. We found that monocyte-intrinsic IL-1α and IL-1β were
390 necessary for control of *Yp* burdens within intestinal PG, consistent with other infectious
391 contexts where hematopoietic-derived IL-1 drives pathogen restriction[62,82]. However, IL-
392 1α and IL-1β production from monocytes was dispensable for control of *Yp* burdens in
393 PG- tissue and systemic organs, suggesting that production from other cell types
394 contribute to IL-1-mediated infection restriction in these compartments. TNFR1 signaling
395 also promoted neutrophil IL-1 production during enteric *Yp* infection, in line with prior
396 studies identifying a role for GSDME-dependent IL-1β production by neutrophils in control
397 of enteric *Yp* infection[48]. Whether neutrophils rely on a similar TNFR1-IL-1 signaling
398 pathway to elicit control of *Yp* remains to be investigated.

399 Finally, IL-1R on stromal cells was critical for control of *Yp* infection. In other
400 infectious contexts, IL-1R signaling in stromal cells is important for pathogen control,
401 highlighting a recurring theme of IL-1R signaling cross-talk between immune and non-
402 immune cells during infection[62,64,68,88,89]. Stromal cells are increasingly appreciated as
403 critical components of the innate immune response. IL-1R is expressed in non-lymphoid
404 tissues, including epithelial and endothelial cells, across various organs[90], suggesting a
405 conserved mechanism by which hematopoietic cytokine signaling can be amplified during
406 infection and inflammation. The stromal cells in the intestine that respond to IL-1R
407 signaling and the downstream anti-bacterial functions that promote restriction of *Yersinia*
408 remain unknown. Intestinal epithelial cells respond to IL-1R signaling by upregulating
409 antimicrobial peptide production, promoting neutrophil recruitment, and modulating
410 intestinal permeability[59,64,69,70,89,91,92]. Neutrophil activation is critical within intestinal PG

411 during *Yersinia* infection and decreased neutrophil recruitment is observed in the absence
412 of monocytes[25] and TNFR1 signaling. Whether IL-1R signaling on the intestinal epithelial
413 or endothelial compartment promotes neutrophil recruitment and function during *Yp*
414 infection remains to be determined in future studies. Altogether, our work uncovers a
415 monocyte-intrinsic TNF/IL-1 circuit that signals to IL-1R on stromal cells to control
416 *Yersinia* infection, providing new mechanistic insight into the cytokine networks that
417 promote enteric granuloma formation and function.

Methods

Mice

C57BL/6J (CD45.2), C57BL/6.SJL (CD45.1), *Ccr2*$^{gfp/gfp}$ mice[93] were obtained from the Jackson Laboratory. *Tnfr1*$^{-/-}$ [94], *Ripk1*^{K45A} [95], *Il1r1*$^{-/-}$ [96], *Il1a*$^{-/-}$[97], *Il1b*$^{-/-}$[97] and *Il1a*$^{-/-}$*Il1b*$^{-/-}$ [97] mice were previously described. All mice were bred at the University of Pennsylvania by homozygous mating and housed separately by genotype. Mice of either sex between 8-12 weeks of age were used for all experiments. All animal studies were performed in strict accordance with University of Pennsylvania Institutional Animal Care and Use Committee-approved protocols (protocol #804523).

Bacteria

Wild-type *Yp* (clinical isolate strain 32777, serogroup O1)[98] and isogenic YopJ-deficient mutant were provided by Dr. James Bliska (Dartmouth College) and previously described[47]. Generation of mutants lacking YopE (*ΔyopE*), enzymatic activity of YopH (YopH^{R409A}), or both (denoted *yopEH*) were previously described[25].

Bone marrow chimeras

Wild-type B6.SJL mice (CD45.1 background) or knockout mice (*Tnfr1*$^{-/-}$ or *Il1r1*$^{-/-}$, CD45.2 background) were lethally irradiated (1096 rads). 6 hours later, mice were injected retro-orbitally with freshly isolated bone marrow cells (5x10^6 total cells, 2.5x10^6 cells per donor in mixed groups) from isogenic donors of the indicated genotypes. All chimeras were provided with antibiotic-containing acidified water (40 mg trimethoprim and 200 mg sulfamethoxazole per 500 mL drinking water) for four weeks after irradiation and

441 subsequently provided acidified water without antibiotics for a total of at least ten weeks.
442 The reconstitution of hematopoietic cells (proportion of donor $CD45^+$ cells among total
443 $CD45^+$ cells) in the blood, spleen, or intestine was analyzed by flow cytometry.
444
445 *Mouse infections*
446 *Yp* was cultured to stationary phase at 28°C and 250 rpm shaking for 16 hours in
447 2xYT broth supplemented with 2 μg/ml triclosan (Millipore Sigma). Mice were fasted for
448 16 hours and subsequently inoculated by oral gavage with 200 μl phosphate-buffered
449 saline (PBS) as previously[25] All bacterial strains were administered at $2x10^8$ colony-
450 forming units (CFU) per mouse.
451
452 *Bacterial CFU quantifications*
453 Tissues were collected in sterile PBS, weighed, homogenized for 40 seconds with
454 6.35 mm ceramic spheres (MP Biomedical) using a FastPrep-24 bead beater (MP
455 Biomedical). Samples were serially diluted tenfold in PBS, plated on LB agar
456 supplemented with 2 μg/ml triclosan, and incubated for two days at room temperature.
457 Dilutions of each sample were plated in triplicate and expressed as the mean CFU per
458 gram or per biopsy.
459
460 *Cytokine quantification*
461 Cytokines were measured in homogenized tissue supernatants using a Cytometric
462 Bead Array (BD Biosciences) according to manufacturer's instructions with the following
463 modification: the amounts of capture beads, detection reagents, and sample volumes

464 were scaled down tenfold. Data were collected on an LSRFortessa flow cytometer (BD
465 Biosciences) and analyzed with FlowJo v10 (BD Biosciences).
466
467 *Tissue preparation and cell isolation*
468 Blood was harvested by cardiac puncture upon euthanasia and collected in 250
469 U/ml Heparin solution (Millipore Sigma). Erythrocytes were lysed with Red Blood Cell
470 Lysing Buffer (Millipore Sigma).
471 Spleens were homogenized through a 70 µm cell strainer (Fisher Scientific), then
472 flushed with R10 buffer consisting of RPMI 1640 (Millipore Sigma) supplemented with 10
473 mM HEPES (Millipore Sigma), 10% fetal bovine serum (Omega Scientific), 1 mM sodium
474 pyruvate (Thermo-Fisher Scientific), and 100 U/ml penicillin + 100 µg/ml streptomycin
475 (Thermo Fisher Scientific). Erythrocytes were lysed with Red Blood Cell Lysing Buffer
476 (Millipore Sigma).
477 Intestines were excised, flushed luminally with sterile PBS to remove the feces,
478 opened longitudinally along the mesenteric side and placed luminal side down on cutting
479 boards (Epicurean). Small intestinal tissue containing macroscopically visible
480 pyogranulomas (PG+), adjacent non-granulomatous areas (PG-) and uninfected control
481 tissue (uninf) were excised using a 2 mm-ø dermal punch-biopsy tool (Keyes). Biopsies
482 within each mouse were pooled groupwise, suspended in epithelial dissociation buffer
483 consisting of calcium and magnesium-free HBSS (Thermo Fisher Scientific)
484 supplemented with 15 mM HEPES, 10 mg/ml bovine serum albumin (Millipore Sigma), 5
485 mM EDTA (Millipore Sigma), and 100 U/ml penicillin + 100 µg/ml streptomycin, then
486 incubated for 30 minutes at 37°C under continuous agitation at 300 RPM. To isolate

immune cells from the lamina propria, the tissue was enzymatically digested in R10 buffer, along with 0.5 Wünsch units/ml liberase TM (Roche), 30 µg/ml DNase I (Roche), and 5 mM $CaCl_2$ for 20 min at 37°C under continuous agitation. The resulting cell suspensions were filtered through 100 µm cell strainers (Fisher Scientific) and subjected to density gradient centrifugation using Percoll (GE Healthcare). Briefly, cells were suspended in 40% Percoll and centrifuged over a 70% Percoll layer for 20 min at 600 × g with the lowest brake at room temperature. Cells collected between the layers were washed with R10 buffer for downstream analysis.

Flow cytometry

Non-specific Fc binding was blocked for 10 minutes on ice with unconjugated anti-CD16/CD32 (93; Thermo-Fisher Scientific). Cells were subsequently labeled for 30 minutes on ice with the following antibodies and reagents: PE-conjugated rat anti-mouse Siglec-F (E50-2440; BD Biosciences), PE-TxR or PE-Cy5-conjugated rat anti-mouse CD11b (M1/70.15; Thermo Fisher Scientific), PE-Cy5.5 or PE-Cy7-conjugated rat anti-mouse CD4 (RM4-5; Thermo Fisher Scientific), BV510-conjugated rat anti-mouse CD3e (145-2C11; BioLegend), AF700 or PerCP-Cy5.5-conjugated rat anti-mouse Ly-6C (HK1.4; Thermo Fisher Scientific), BV605-conjugated Armenian hamster anti-mouse TCRβ (H57-597; BD Biosciences), BV650-conjugated rat anti-mouse I-A/I-E (M5/114.15.2; BD Biosciences), BV711-conjugated rat anti-mouse CD8α (53-6.7; BD Biosciences), BV785-conjugated rat anti-mouse Ly-6G (1A8; Thermo Fisher Scientific), PE-Cy7 or AF647-conjugated mouse anti-mouse CD64 (X54-5/7.1; BD Biosciences), AF700-conjugated mouse anti-mouse CD45.2 (104; BioLegend), PE-Cy5-conjugated

mouse anti-mouse CD45.1 (A20; Thermofisher), PE-Cy5 or PE-CF594-conjugated rat anti-mouse CD45R/B220 (RA3-6B2; BD Biosciences) along with eF780 viability dye (BioLegend) diluted in PBS. Antibodies were used at 1:200 dilution and viability dye at 1:1500 dilution.

For intracellular staining, cells were incubated for 3 hours at 37°C with 5% CO_2 in R10 buffer supplemented with 0.33 µl/ml GolgiStop (BD Biosciences) and 15 µg/ml DNase I. Surface proteins were stained as above, and cells were fixed for 20 minutes on ice with Cytofix/Cytoperm Fixation/Permeabilization solution (BD Biosciences). Intracellular cytokines were stained at 4°C overnight with FITC or PerCP-e710-conjugated rat anti-mouse IL-1β (NJTEN3; Thermo Fisher Scientific) and PE-conjugated Armenian hamster anti-mouse IL-1α (ALF-161; BioLegend). All intracellular antibodies were diluted 1:200 in Perm/Wash Buffer (BD Biosciences). Cells were acquired on an LSRFortessa flow cytometer and data were analyzed with FlowJo v10. Cells were gated on live singlets prior to downstream analyses.

Histology

Tissues were fixed in 10% neutral-buffered formalin (Fisher Scientific) and stored at 4°C until further processed. Tissue pieces were embedded in paraffin, sectioned by standard histological techniques and stained with hematoxylin and eosin. Slides were scanned on an Aperio VERSA using brightfield at 20x magnification. Histopathological disease scoring was performed by blinded board-certified pathologists. Tissue sections were given a score from 0-4 (healthy-severe) for multiple parameters, including degree

532 of inflammatory cell infiltration, necrosis, and free bacterial colonies, along with tissue-
533 specific parameters such as villus blunting and crypt hyperplasia.
534
535 *Statistics*
536 Statistical analyses were performed using Prism v9.0 (GraphPad Software).
537 Independent groups were compared by Mann-Whitney U test or Kruskal-Wallis test with
538 Dunn's multiple comparisons test. Survival curves were compared by Mantel-Cox test.
539 Statistical significance is denoted as * ($p<0.05$), ** ($p<0.01$), *** ($p<0.001$), ****
540 ($p<0.0001$), or ns (not significant).

Figure legends

Figure 1. TNFR1 is required for organized pyogranuloma formation and restriction of *Yersinia* in intestine and periphery

(**A**) H&E-stained paraffin-embedded longitudinal small intestinal sections from *Yp*-infected mice at day 5 post-infection. Dashed line highlights pyogranuloma (left) or necrosuppurative lesion (right). Images representative of two independent experiments. Scale bars = 500 μm (top) and 200 μm (bottom).

(**B**) Histopathological scores of small intestinal tissue from uninfected or *Yp*-infected mice at day 5 post-infection. Each mouse was scored between 0-4 (healthy-severe) for indicated sign of pathology. Each circle represents one mouse. Lines represent median. Pooled data from two independent experiments.

(**C**) Bacterial burdens in small intestinal PG- and PG+ tissue isolated day 5 post-infection. Each circle represents the mean CFU of 3-5 pooled punch biopsies from one mouse. Lines represent geometric mean. Pooled data from three independent experiments.

(**D**) Total numbers and frequencies of $CD45^+$ cells, monocytes, macrophages, and neutrophils in uninfected, PG-, and PG+ small intestinal tissue isolated 5 days post-infection. Each circle represents the mean of 3-10 pooled punch biopsies from one mouse. Lines represent median. Pooled data from three independent experiments.

(**E**) Mean fluorescence intensity (MFI) of CD11b expression on neutrophils in PG+ tissue at day 5 post-infection. Each circle represents the mean of 3-10 pooled punch biopsies from one mouse. Lines represent median. Data representative of three independent experiments.

(**F**) Bacterial burdens in indicated organs at day 5 post-infection. Each circle represents one mouse. Lines represent geometric mean. Pooled data from four independent experiments.

(**G**) Survival of infected WT (n=9) and *Tnfr1*$^{-/-}$ (n=21) mice. Pooled data from two independent experiments.

(**H**) Bacterial burdens in small intestinal PG- and PG+ tissue at day 5 post-infection of indicated chimeric mice. Each circle represents the mean *Yp*-CFU of 3-5 pooled punch biopsies from one mouse. Lines represent geometric mean. Pooled data from two independent experiments.

(**I**) Bacterial burdens in indicated organs at day 5 post-infection of indicated chimeric mice. Each circle represents one mouse. Lines represent geometric mean. Pooled data from two independent experiments.

Statistical analysis by Mann-Whitney U test (B, C, D, E, F), Mantel-Cox test (G), and Kruskal-Wallis test with Dunn's multiple comparisons correction (H, I) *p<0.05, **p<0.01, ***p<0.001, ****p<0.0001, ns = not significant.

Figure 2. Autocrine TNF signaling in monocytes is required for control of *Yersinia*

(**A**) Schematic of mixed bone marrow chimeras.

(**B**) H&E-stained paraffin-embedded transverse small-intestinal sections from chimeric WT mice reconstituted with *Ccr2*$^{gfp/gfp}$ + *WT* (left), *Ccr2*$^{gfp/gfp}$ + *Tnfr1*$^{-/-}$ (middle), or *Ccr2*$^{gfp/gfp}$ (right) bone marrow, at day 5 post-infection. Dotted lines highlight lesions. Scale bars = 100 µm. Images representative of two independent experiments.

(**C**) Bacterial burdens in small intestinal PG- and PG+ tissue of chimeric WT mice reconstituted with either *Ccr2*$^{gfp/gfp}$ + *WT* (white), *Ccr2*$^{gfp/gfp}$ + *Tnfr1*$^{-/-}$ (light gray), or *Ccr2*$^{gfp/gfp}$ (dark gray) at day 5 post *Yp*-infection. Each symbol represents one mouse. Lines represent geometric mean. Pooled data from two independent experiments.

(**D**) Bacterial burdens in indicated organs at day 5 post-infection. Each circle represents one mouse. Lines represent geometric mean. Pooled data from two independent experiments.

(**E**) Bacterial burdens in small intestinal PG- and PG+ tissue of chimeric WT mice reconstituted with either *Tnf*$^{-/-}$ + *WT* (white), *Tnf*$^{-/-}$ + *Ccr2*$^{gfp/gfp}$ (light gray), or *Tnf*$^{-/-}$ (dark gray) at day 5 post *Yp*-infection. Each symbol represents one mouse. Lines represent geometric mean. Pooled data from three independent experiments.

(**F**) Bacterial burdens in indicated organs at day 5 post-infection. Each circle represents one mouse. Lines represent geometric mean. Pooled data from three independent experiments.

Statistical analysis by Kruskal-Wallis test with Dunn's multiple comparisons correction. *p<0.05, **p<0.01, ***p<0.001, ****p<0.0001, ns = not significant.

Figure 3. TNFR1 signaling in monocytes controls *Yp* infection independently of RIPK1 kinase-induced cell death

(**A**) Bacterial burdens in small intestinal PG- and PG+ tissue of WT (white) and *Ripk1*^{K45A} (blue) mice at day 5 post *Yp*-infection. Each symbol represents one mouse. Lines represent geometric mean. Pooled data from two independent experiments.

(**B**) Bacterial burdens in indicated organs at day 5 post-infection. Each circle represents one mouse. Lines represent geometric mean. Pooled data from two independent experiments.

(**C**) H&E-stained paraffin-embedded longitudinal small intestinal sections from WT (left) and *Ripk1*^{K45A} (right) mice at day 5 post *Yp*-infection with dotted line highlighting lesion. Scale bars = 100 μm. Representative images of two independent experiments.

(**D**) H&E-stained paraffin-embedded transverse small-intestinal sections from chimeric WT mice reconstituted with either *Ccr2*$^{gfp/gfp}$ + WT (left), *Ccr2*$^{gfp/gfp}$ + *Ripk1*^{K45A} (middle), or *Ccr2*$^{gfp/gfp}$ (right) bone marrow, at day 5 post *Yp*-infection with dotted line highlighting lesion. Scale bars = 100 μm. Representative images of two independent experiments.

(**E**) Bacterial burdens in small intestinal PG- and PG+ tissue of chimeric WT mice reconstituted with either *Ccr2*$^{gfp/gfp}$ + *WT* (white), *Ccr2*$^{gfp/gfp}$ + *Ripk1*^{K45A} (light gray), or *Ccr2*$^{gfp/gfp}$ (dark gray) at day 5 post *Yp*-infection. Each symbol represents one mouse. Lines represent geometric mean. Pooled data from two independent experiments.

(**F**) Bacterial burdens in indicated organs at day 5 post-infection. Each circle represents one mouse. Lines represent geometric mean. Pooled data from two independent experiments.

(**G**) H&E-stained paraffin-embedded longitudinal small intestinal sections from WT and *Tnfr1*$^{-/-}$ mice infected with either WT or Δ*yopJ Yp* at day 5 post-infection. Scale bars = 100 μm. Representative images of three independent experiments.

(**H**) Bacterial burdens in indicated organs at day 5 post-infection. Each circle represents one mouse. Lines represent geometric mean. Pooled data from four independent experiments.

(**I**) Survival of WT (white) and *Tnfr1*$^{-/-}$ (gray) mice infected with WT (circles) or *ΔyopJ* (squares) *Yp*. n = 9-12 mice per group. Pooled data from two independent experiments.
(**J**) Survival of WT (white) or *Tnfr1*$^{-/-}$ (gray) mice infected with WT (circles) or *yopEH* (squares) *Yp*. n = 11-15 mice per group. Pooled data from two independent experiments.
Statistical analysis by Mann-Whitney U test (A, B), Kruskal-Wallis test with Dunn's multiple comparisons correction (E, F, H), or Mantel-Cox test (I, J). *p<0.05, **p<0.01, ***p<0.001, ****p<0.0001, ns = not significant.

Figure 4. Cell-intrinsic TNFR1 signaling is required for maximal IL-1 production within intestinal pyogranulomas during *Yersinia* infection

(**A**) Cytokine levels were measured by cytometric bead array in tissue punch biopsy homogenates isolated 5 days post-infection from chimeric WT mice reconstituted with indicated donor cells. Lines represent median. Pooled data from two independent experiments.
(**B**) Intracellular cytokine levels in monocytes and neutrophils isolated from small intestinal PG+ tissue 5 days post-infection. Each circle represents the mean of 3-10 pooled punch biopsies from one mouse. Lines represent median. Pooled data from three independent experiments.
(**C**) Flow cytometry plots of intracellular IL-1 in monocytes (CD64^{+} Ly-6C^{hi}) from small intestinal PG+ tissue at day 5 post-infection. Plots representative of two independent experiments.
(**D**) Aggregate datasets from (C) for intracellular IL-1 staining in monocytes and neutrophils in small intestinal PG+ tissue at day 5 post-infection. Each circle represents

653 the mean of 3-10 pooled punch biopsies from one mouse. Lines connect congenic cell
654 populations within individual mice. Pooled data from two independent experiments.
655 Statistical analysis by Kruskal-Wallis test with Dunn's multiple comparisons correction
656 (A), Mann-Whitney U test (B), congenic cells within mice: Wilcoxon test; across groups:
657 Mann-Whitney U test (D). *p<0.05, **p<0.01, ***p<0.001, ****p<0.0001, ns = not
658 significant.
659
660 **Figure 5. IL-1 signaling is required for organized pyogranuloma formation and**
661 **intestinal control of *Yersinia***
662 (**A**) Bacterial burdens in small intestinal Peyer's patches (PP), PG-, and PG+ tissues
663 isolated 5 days post-infection. For PP, each circle represents pooled tissue from one
664 mouse. For PG- and PG+, each circle represents the mean of 3-5 pooled punch biopsies
665 from one mouse. Lines represent geometric mean. Pooled data from three independent
666 experiments.
667 (**B**) H&E-stained paraffin-embedded longitudinal small intestinal sections from *Yp*-
668 infected mice at day 5 post-infection. Representative images of one experiment. Scale
669 bars = 250 µm.
670 (**C**) Survival of infected WT (n=26) and *Il1r1*$^{-/-}$ (n=20) mice. Pooled data from two
671 independent experiments
672 (**D**). Bacterial burdens in small intestinal PP, PG-, and PG+ tissues at day 5 post-infection
673 of indicated genotypes. For PP, each circle represents pooled tissue from one mouse.
674 For PG- and PG+, each circle represents the mean of 3-5 pooled punch biopsies from

675 one mouse. Lines represent geometric mean. Pooled data from three independent
676 experiments.
677 (**E**). Survival of infected WT (n=27, n=19), *Il1a*$^{-/-}$ (n=22), and *Il1b*$^{-/-}$ (n=21) mice. Pooled
678 data from three (WT vs *Il1a*$^{-/-}$) and two (WT vs *Il1b*$^{-/-}$) independent experiments.
679 Statistical analysis by Mann-Whitney U test (A, D) or Mantel-Cox test (C, E) *p<0.05,
680 **p<0.01, ****p<0.0001, ns = not significant.
681
682 **Figure 6. Monocyte-derived IL-1 signals to nonhematopoietic cells to restrict**
683 ***Yersinia* infection in intestinal pyogranulomas**
684 (**A**) Bacterial burdens in small intestinal Peyer's patches (PP), PG-, and PG+ tissues at
685 day 5 post-infection of indicated chimeric mice. For PP, each circle represents pooled
686 tissue from one mouse. For PG- and PG+, each circle represents the mean of 3-5 pooled
687 punch biopsies from one mouse. Lines represent geometric mean. Data pooled from two
688 independent experiments.
689 (**C**) Bacterial burdens in small intestinal Peyer's patches (PP), PG-, and PG+ tissues
690 isolated 5 days post-infection of indicated chimeric mice. For PP, each circle represents
691 one mouse. For PG- and PG+, each circle represents the mean of 3-5 pooled punch
692 biopsies from one mouse. Lines represent geometric mean. Pooled data from three
693 independent experiments.
694 (**C**) Bacterial burdens in indicated organs at day 5 post-infection of indicated chimeric
695 mouse. Each circle represents one mouse. Lines represent geometric mean. Data pooled
696 from three independent experiments.

(**D**) Model of TNF-IL-1 circuit mediated by monocyte and stromal compartment to promote *Yp* restriction within intestinal pyogranulomas.

All statistical analysis by Kruskal-Wallis test with Dunn's multiple comparisons correction. *p<0.05, **p<0.01, ***p<0.001, ns = not significant.

Supplemental Figure 1. Effects of TNFR1-deficiency on pyogranuloma formation in intestine and lymphatic tissue during *Yersinia* infection

(A) Total number of intestinal lesions at day 5 post-infection with *Yp*. Each circle represents one mouse. Lines represent median. Pooled data from four independent experiments.

(B) Flow cytometry plots displaying the gating strategy employed to identify neutrophils (CD11b+ Ly-6G+), monocytes ($CD64^+$ $Ly\text{-}6C^{hi}$), and macrophages ($CD64^+$ $Ly\text{-}6C^{lo}$ $MHC\text{-}II^{hi}$) in small intestinal PG+ tissue. Representative images of three independent experiments.

(C) Frequencies of indicated cell types in blood of uninfected chimeric mice. Pooled data from two independent experiments.

All statistical analyses by Mann-Whitney U test. *p<0.05, **p<0.01, ***p<0.001, ****p<0.0001, ns = not significant.

Supplemental Figure 2. Autocrine TNF signaling in monocytes is required for systemic control of *Yersinia*

(A) Frequency of indicated cell types in the blood of uninfected chimeric mice.

(B) Bacterial burdens in indicated organs at day 5 post-infection. Each circle represents one mouse. Lines represent geometric mean.

(C) Bacterial burdens in small-intestinal PG- and PG+ tissue at day 5 post *Yp*-infection. Each symbol represents one mouse. Lines represent geometric mean.

All data pooled from two independent experiments. Statistical analysis by Kruskal-Wallis test with Dunn's multiple comparisons correction. Mann-Whitney U test. *p<0.05, **p<0.01, ***p<0.001, ****p<0.0001, ns = not significant.

Supplemental Figure 3. TNFR1 signalling in monocytes is independent of YopJ-induced RIPK1 kinase activity

(**A**) Frequency of indicated cell types in the blood of uninfected chimeric mice.

(**B**) Survival of *wild-type* (left) and *Tnfr1*$^{-/-}$ (right) mice infected with WT (white circles), *ΔyopE* (blue) or YopH^{R409A} (white squares) *Yp*. n = 5-32 (*wild-type*) and 13-20 (*Tnfr1*$^{-/-}$) mice per group. Pooled data from 2-4 independent experiments.

Statistical analysis by Mantel-Cox test (B). *p<0.05, **p<0.01, ***p<0.001, ****p<0.0001, ns = not significant.

Supplemental Figure 4. Cytokine production downstream of TNFR1 expression on monocytes is specific to IL-1 in intestinal pyogranulomas

(**A**) Cytokine levels in homogenates of tissue punch biopsies were measured by cytometric bead array at day 5 post-infection of chimeric WT mice reconstituted with indicated cells. Lines represent median. Pooled data from two independent experiments.

(**B**) Cytokine levels in serum were measured by cytometric bead array at day 5 post-infection of chimeric WT mice reconstituted with indicated cells. Lines represent median. ND = not detected. Pooled data from two independent experiments.

(**C**) Frequencies of indicated cell types in small intestinal PG+ tissue or spleen at day 5 post-infection of WT chimeric mice reconstituted with the indicated cells. Pooled data from two independent experiments.

(**D**) Flow cytometry plots of intracellular IL-1 in monocytes ($CD64^+$ Ly-$6C^{hi}$) from small intestinal PG+ tissue in WT and *Il1b*$^{-/-}$ mice at day 5 post-infection. Plots representative of two independent experiments.

(**E**) Intracellular levels of TNF in monocytes and neutrophils in small intestinal PG+ tissue at day 5 post-infection. Each circle represents the mean of 3-10 pooled punch biopsies from one mouse. Lines connect congenic cell populations within individual mice. Pooled data from two independent experiments.

Statistical analyses by Kruskal-Wallis test with Dunn's multiple comparisons correction (A, B), or congenic cells within mice: Wilcoxon test; across groups: Mann-Whitney U test (E). ns = not significant.

Supplemental Figure 5. Systemic bacterial burdens are comparable in WT and IL-1-deficient mice.

Bacterial burdens in indicated organ at day 5 post-infection. Each circle represents one mouse. Lines represent geometric mean. Pooled data from three independent experiments.

All statistical analyses by Mann-Whitney U test. *$p<0.05$, ns = not significant.

Supplemental Figure 6. Monocyte-derived IL-1 signals to non-hematopoietic cells to restrict *Yersinia* infection

(**A**) Frequencies of cell types in the blood of chimeric mice. Pooled data from two independent experiments

(**B**) Bacterial burdens in indicated organ at day 5 post-infection of indicated chimeric mouse. Each circle represents one mouse. Lines represent geometric mean. Pooled data from two independent experiments.

(**C**) Frequencies of indicated cell types in small intestinal PG+ tissue at day 5 post-infection of indicated chimeric mouse. Pooled data from three independent experiments

Statistical analysis by Kruskal-Wallis test with Dunn's multiple comparisons correction (B). *$p<0.05$, ns = not significant.

Acknowledgements

We thank Enrico Radaelli for constructive input and the staff at the PennVet Comparative Pathology Core for their help in preparing and analyzing the histological samples. We thank members of the Brodsky and Shin labs for scientific discussion. This work was supported by NIH Awards R01AI128530 (IEB), R01AI1139102A1 (IEB), and R01DK123528 (IEB); BWF Investigator in the Pathogenesis of Infectious Disease Award (IEB, SS); Mark Foundation Grant 19-011MIA (IEB), the Foundation Blanceflor Postdoctoral Scholarship (DS), the Swedish Society for Medical Research postdoctoral fellowship (DS) and the Sweden-America Foundation J. Sigfrid Edström award (DS); NIH NRSA F31AI160741-01 (RM); NIH T32 AI141393-2 (RM); F32 AI164655 (JPG); NIH NRSA F31AI161319 (BH); and NSF GRFP Award (SP); NIH T32 AI141393-03 (JZ); NIH Awards R21AI151476 (SS), R01AI118861 (SS), and R01AI123243 (SS). The veterinary pathologists performing the histopathological analysis are supported by the Abramson Cancer Center Support Grant (P30 CA016520). The scanner used for whole slide imaging and the image visualization software was supported by an NIH Shared Instrumentation Grant (S10 OD023465-01A1). Model figure was created using Biorender.

Competing interests

The authors have no conflicting financial interests.

Abbreviations

CCR2	CC chemokine receptor 2
MLN	Mesenteric lymph nodes
PG	Pyogranuloma
PP	Peyer's patches
RIPK1	Receptor-interacting protein kinase 1
TNF	Tumor necrosis factor
TNFR1	Tumor necrosis factor receptor 1
Yp	Yersinia pseudotuberculosis
Yop	Yersinia outer protein

804 **References**

805 1. Pagán, A. J. & Ramakrishnan, L. The Formation and Function of Granulomas.
806 *https://doi.org/10.1146/annurev-immunol-032712-100022* **36**, 639–665 (2018).
807 2. Petersen, H. J. & Smith, A. M. The role of the innate immune system in
808 granulomatous disorders. *Front. Immunol.* **4**, (2013).
809 3. Diedrich, C. R., O'Hern, J. & Wilkinson, R. J. HIV-1 and the Mycobacterium
810 tuberculosis granuloma: A systematic review and meta-analysis. *Tuberculosis* **98**,
811 62–76 (2016).
812 4. Davis, J. M. & Ramakrishnan, L. The role of the granuloma in expansion and
813 dissemination of early tuberculous infection. *Cell* **136**, 37–49 (2009).
814 5. Adams, K. N. *et al.* Drug tolerance in replicating mycobacteria mediated by a
815 macrophage-induced efflux mechanism. *Cell* **145**, 39–53 (2011).
816 6. Kindler, V., Sappino, A. P., Grau, G. E., Piguet, P. F. & Vassalli, P. The inducing
817 role of tumor necrosis factor in the development of bactericidal granulomas during
818 BCG infection. *Cell* **56**, 731–740 (1989).
819 7. Algood, H. M. S., Lin, P. L. & Flynn, J. A. L. Tumor necrosis factor and chemokine
820 interactions in the formation and maintenance of granulomas in tuberculosis. *Clin.*
821 *Infect. Dis.* **41 Suppl 3**, (2005).
822 8. Chakravarty, S. D. *et al.* Tumor necrosis factor blockade in chronic murine
823 tuberculosis enhances granulomatous inflammation and disorganizes granulomas
824 in the lungs. *Infect. Immun.* **76**, 916–926 (2008).
825 9. Lin, P. L. *et al.* TNF neutralization results in disseminated disease during acute
826 and latent *M. tuberculosis* infection with normal granuloma structure. *Arthritis*

Rheum. **62**, NA-NA (2010).

10. Flynn, J. L. *et al. Tumor Necrosis Factor-u Is Required in the Protective Immune Response Against Mycobacterium tuberculosis in Mice*. *Immunity* vol. 2 (1995).

11. Bean, A. G. *et al.* Structural deficiencies in granuloma formation in TNF gene-targeted mice underlie the heightened susceptibility to aerosol Mycobacterium tuberculosis infection, which is not compensated for by lymphotoxin. *J. Immunol.* **162**, 3504–11 (1999).

12. Roach, D. R. *et al.* TNF Regulates Chemokine Induction Essential for Cell Recruitment, Granuloma Formation, and Clearance of Mycobacterial Infection. *J. Immunol.* **168**, 4620–4627 (2002).

13. Clay, H., Volkman, H. E. & Ramakrishnan, L. Tumor necrosis factor signaling mediates resistance to mycobacteria by inhibiting bacterial growth and macrophage death. *Immunity* **29**, 283–294 (2008).

14. Takeda, K. & Akira, S. TLR signaling pathways. *Semin. Immunol.* **16**, 3–9 (2004).

15. Chen, G. & Goeddel, D. V. TNF-R1 signaling: a beautiful pathway. *Science* **296**, 1634–1635 (2002).

16. Kusnadi, A. *et al.* The Cytokine TNF Promotes Transcription Factor SREBP Activity and Binding to Inflammatory Genes to Activate Macrophages and Limit Tissue Repair. *Immunity* **51**, 241-257.e9 (2019).

17. T, A. *et al.* Clinical use of anti-TNF therapy and increased risk of infections. *Drug. Healthc. Patient Saf.* **5**, 79 (2013).

18. El-Maraghi, N. R. H. & Mair, N. S. The Histopathology of Enteric Infection with Yersinia pseudotuberculosis. *Am. J. Clin. Pathol.* **71**, 631–639 (1979).

19. Lamps, L. W. *et al.* The role of Yersinia enterocolitica and Yersinia pseudotuberculosis in granulomatous appendicitis: a histologic and molecular study. *Am. J. Surg. Pathol.* **25**, 508–15 (2001).

20. Kojima, M. *et al.* Immunohistological findings of suppurative granulomas of Yersinia enterocolitica appendicitis: a report of two cases. *Pathol. Res. Pract.* **203**, 115–119 (2007).

21. Rohena, F. J., Almira-Suárez, M. I. & González-Keelan, C. Granulomatous enterocolitis secondary to Yersinia in an 11-year-old boy from Puerto Rico, confirmed by PCR: a case report. *P. R. Health Sci. J.* **33**, 27–30 (2014).

22. Richardson, T., Jones, M., Akhtar, Y. & Pollard, J. Suspicious Yersinia granulomatous enterocolitis mimicking appendicitis. *BMJ Case Rep.* **2018**, (2018).

23. Zhang, Y., Khairallah, C., Sheridan, B. S., van der Velden, A. W. M. & Bliska, J. B. CCR2+ Inflammatory Monocytes Are Recruited to Yersinia pseudotuberculosis Pyogranulomas and Dictate Adaptive Responses at the Expense of Innate Immunity during Oral Infection. *Infect. Immun.* **86**, (2018).

24. Davis, K. M., Mohammadi, S. & Isberg, R. R. Community behavior and spatial regulation within a bacterial microcolony in deep tissue sites serves to protect against host attack. *Cell Host Microbe* **17**, 21–31 (2015).

25. Sorobetea, D. *et al.* Inflammatory monocytes promote granuloma control of Yersinia infection. *Nat. Microbiol.* 1–13 (2023) doi:10.1038/s41564-023-01338-6.

26. Atkinson, S. & Williams, P. Yersinia virulence factors - a sophisticated arsenal for combating host defences. *F1000Research* **5**, 1370 (2016).

27. Bliska, J. B., Brodsky, I. E. & Mecsas, J. Role of the Yersinia pseudotuberculosis

Virulence Plasmid in Pathogen-Phagocyte Interactions in Mesenteric Lymph Nodes. *EcoSal Plus* **9**, (2021).

28. Autenrieth, I. B. & Heesemann, J. In vivo neutralization of tumor necrosis factor-alpha and interferon-gamma abrogates resistance to Yersinia enterocolitica infection in mice. *Med. Microbiol. Immunol.* **181**, 333–338 (1992).

29. Parent, M. A. *et al.* Gamma interferon, tumor necrosis factor alpha, and nitric oxide synthase 2, key elements of cellular immunity, perform critical protective functions during humoral defense against lethal pulmonary Yersinia pestis infection. *Infect. Immun.* **74**, 3381–3386 (2006).

30. Peterson, L. W. *et al.* Cell-Extrinsic TNF Collaborates with TRIF Signaling To Promote Yersinia-Induced Apoptosis. *J. Immunol.* **197**, 4110–4117 (2016).

31. Borjesson, D. L., Simon, S. I., Hodzic, E., Ballantyne, C. M. & Barthold, S. W. Kinetics of CD11b/CD18 Up-Regulation During Infection with the Agent of Human Granulocytic Ehrlichiosis in Mice. *Lab. Investig. 2002 823* **82**, 303–311 (2002).

32. Mann, B. S. & Chung, K. F. Blood neutrophil activation markers in severe asthma: Lack of inhibition by prednisolone therapy. *Respir. Res.* **7**, 1–10 (2006).

33. Yoon, J. W., Pahl, M. V. & Vaziri, N. D. Spontaneous leukocyte activation and oxygen-free radical generation in end-stage renal disease. *Kidney Int.* **71**, 167–172 (2007).

34. Pham, T. H. M. *et al.* Salmonella-Driven Polarization of Granuloma Macrophages Antagonizes TNF-Mediated Pathogen Restriction during Persistent Infection. *Cell Host Microbe* **27**, 54-67.e5 (2020).

35. Peterson, L. W. *et al.* RIPK1-dependent apoptosis bypasses pathogen blockade

of innate signaling to promote immune defense. *J. Exp. Med.* **214**, 3171–3182 (2017).

36. Ea, C. K., Deng, L., Xia, Z. P., Pineda, G. & Chen, Z. J. Activation of IKK by TNFalpha requires site-specific ubiquitination of RIP1 and polyubiquitin binding by NEMO. *Mol. Cell* **22**, 245–257 (2006).

37. Christofferson, D. E., Li, Y. & Yuan, J. Control of Life-or-Death Decisions by RIP1 Kinase. *https://doi.org/10.1146/annurev-physiol-021113-170259* **76**, 129–150 (2014).

38. Ofengeim, D. & Yuan, J. Regulation of RIP1 kinase signalling at the crossroads of inflammation and cell death. *Nat. Rev. Mol. Cell Biol.* **14**, 727–736 (2013).

39. Weinlich, R. & Green, D. R. The Two Faces of Receptor Interacting Protein Kinase-1. *Mol. Cell* **56**, 469–480 (2014).

40. Delanghe, T., Dondelinger, Y. & Bertrand, M. J. M. RIPK1 Kinase-Dependent Death: A Symphony of Phosphorylation Events. *Trends Cell Biol.* **30**, 189–200 (2020).

41. Yeap, H. W. & Chen, K. W. RIPK1 and RIPK3 in antibacterial defence. *Biochem. Soc. Trans.* **50**, 1583–1594 (2022).

42. Monack, D. M. *et al.* Yersinia signals macrophages to undergo apoptosis and YopJ is necessary for this cell death. *Proc. Natl. Acad. Sci. U. S. A.* **94**, 10385–90 (1997).

43. Palmer, L. E., Hobbie, S., Galán, J. E. & Bliska, J. B. YopJ of *Yersinia pseudotuberculosis* is required for the inhibition of macrophage TNF-α production and downregulation of the MAP kinases p38 and JNK. *Mol. Microbiol.* **27**, 953–

965 (1998).

44. Orth, K. *et al.* Inhibition of the Mitogen-Activated Protein Kinase Kinase Superfamily by a Yersinia Effector. *Science (80-.).* **285**, 1920–1923 (1999).

45. Yoon, S., Liu, Z., Eyobo, Y. & Orth, K. Yersinia effector YopJ inhibits yeast MAPK signaling pathways by an evolutionarily conserved mechanism. *J. Biol. Chem.* **278**, 2131–2135 (2003).

46. Mukherjee, S. *et al.* Yersinia YopJ acetylates and inhibits kinase activation by blocking phosphorylation. *Science* **312**, 1211–1214 (2006).

47. Philip, N. H. *et al.* Caspase-8 mediates caspase-1 processing and innate immune defense in response to bacterial blockade of NF- B and MAPK signaling. *Proc. Natl. Acad. Sci.* **111**, 7385–7390 (2014).

48. Chen, K. W. *et al.* RIPK1 activates distinct gasdermins in macrophages and neutrophils upon pathogen blockade of innate immune signaling. *Proc. Natl. Acad. Sci. U. S. A.* **118**, (2021).

49. Grosdent, N., Maridonneau-Parini, I., Sory, M. P. & Cornelis, G. R. Role of Yops and adhesins in resistance of Yersinia enterocolitica to phagocytosis. *Infect. Immun.* **70**, 4165–4176 (2002).

50. Green, S. P., Hartland, E. L., M., Robins-Browne, R. M. & Phillips, W. A. Role of YopH in the suppression of tyrosine phosphorylation and respiratory burst activity in murine macrophages infected with Yersinia enterocolitica. *J. Leukoc. Biol.* **57**, 972–977 (1995).

51. Taheri, N., Fahlgren, A. & Fällman, M. Yersinia pseudotuberculosis Blocks Neutrophil Degranulation. *Infect. Immun.* **84**, 3369–3378 (2016).

942 52. Bliska, J. B. & Black, D. S. Inhibition of the Fc receptor-mediated oxidative burst in
943 macrophages by the Yersinia pseudotuberculosis tyrosine phosphatase. *Infect.*
944 *Immun.* **63**, 681–685 (1995).
945 53. Bliska, J. B., Guan, K., Dixon, J. E. & Falkow, S. Tyrosine phosphate hydrolysis of
946 host proteins by an essential Yersinia virulence determinant. *Proc. Natl. Acad.*
947 *Sci.* **88**, 1187–1191 (1991).
948 54. Rosqvist, R., Bolin, I. & Wolf-Watz, H. Inhibition of phagocytosis in Yersinia
949 pseudotuberculosis: a virulence plasmid-encoded ability involving the Yop2b
950 protein. *Infect. Immun.* **56**, 2139–2143 (1988).
951 55. Rosqvist, R., Forsberg, A. & Wolf-Watz, H. Intracellular targeting of the Yersinia
952 YopE cytotoxin in mammalian cells induces actin microfilament disruption. *Infect.*
953 *Immun.* **59**, 4562–4569 (1991).
954 56. Galyov, E. E., Håkansson, S., Forsberg, Å. & Wolf-Watz, H. A secreted protein
955 kinase of Yersinia pseudotuberculosis is an indispensable virulence determinant.
956 *Nature* **361**, 730–732 (1993).
957 57. Black, D. S. & Bliska, J. B. The RhoGAP activity of the Yersinia
958 pseudotuberculosis cytotoxin YopE is required for antiphagocytic function and
959 virulence. *Mol. Microbiol.* **37**, 515–527 (2000).
960 58. Mecsas, J., Raupach, B. & Falkow, S. The Yersinia Yops inhibit invasion of
961 Listeria, Shigella and Edwardsiella but not Salmonella into epithelial cells. *Mol.*
962 *Microbiol.* **28**, 1269–1281 (1998).
963 59. Franchi, L. *et al.* NLRC4-driven production of IL-1β discriminates between
964 pathogenic and commensal bacteria and promotes host intestinal defense. *Nat.*

Immunol. 2012 135 **13**, 449–456 (2012).

60. Barry, K. C., Fontana, M. F., Portman, J. L., Dugan, A. S. & Vance, R. E. IL-1α Signaling Initiates the Inflammatory Response to Virulent Legionella pneumophila In Vivo . *J. Immunol.* (2013) doi:10.4049/jimmunol.1300100.

61. Copenhaver, A. M., Casson, C. N., Nguyen, H. T., Duda, M. M. & Shin, S. IL-1R signaling enables bystander cells to overcome bacterial blockade of host protein synthesis. doi:10.1073/pnas.1501289112.

62. Liu, X., Boyer, M. A., Holmgren, A. M. & Shin, S. Legionella-Infected Macrophages Engage the Alveolar Epithelium to Metabolically Reprogram Myeloid Cells and Promote Antibacterial Inflammation. *Cell Host Microbe* **28**, 683-698.e6 (2020).

63. Fahey, E. & Doyle, S. L. IL-1 family cytokine regulation of vascular permeability and angiogenesis. *Frontiers in Immunology* vol. 10 (2019).

64. Lee, Y.-S. *et al.* Interleukin-1 (IL-1) Signaling in Intestinal Stromal Cells Controls KC/CXCL1 Secretion, Which Correlates with Recruitment of IL-22-Secreting Neutrophils at Early Stages of Citrobacter rodentium Infection. *Infect. Immun.* **83**, 3257–3267 (2015).

65. Vladimer, G. I. *et al.* The NLRP12 Inflammasome Recognizes Yersinia pestis. *Immunity* **37**, 96–107 (2012).

66. Ratner, D. *et al.* Manipulation of Interleukin-1β and Interleukin-18 Production by Yersinia pestis Effectors YopJ and YopM and Redundant Impact on Virulence. *J. Biol. Chem.* **291**, 9894–9905 (2016).

67. Meinzer, U. *et al.* Yersinia pseudotuberculosis effector YopJ subverts the

Nod2/RICK/TAK1 pathway and activates caspase-1 to induce intestinal barrier dysfunction. *Cell Host Microbe* **11**, 337–351 (2012).

68. Bohrer, A. C., Tocheny, C., Assmann, M., Ganusov, V. V. & Mayer–Barber, K. D. Cutting Edge: IL-1R1 Mediates Host Resistance to Mycobacterium tuberculosis by Trans-Protection of Infected Cells. *J. Immunol.* **201**, 1645–1650 (2018).

69. Homaidan, F. R., Chakroun, I., Dbaibo, G. S., El-Assaad, W. & El-Sabban, M. E. IL-1 activates two phospholipid signaling pathways in intestinal epithelial cells. *Inflamm. Res.* (2001) doi:10.1007/PL00000259.

70. Moon, C., Vandussen, K. L., Miyoshi, H. & Stappenbeck, T. S. Development of a primary mouse intestinal epithelial cell monolayer culture system to evaluate factors that modulate IgA transcytosis. *Mucosal Immunol.* **7**, 818–828 (2014).

71. Barnett, K. C. *et al.* An epithelial-immune circuit amplifies inflammasome and IL-6 responses to SARS-CoV-2. *Cell Host Microbe* **31**, (2023).

72. Botha, T. & Ryffel, B. Reactivation of Latent Tuberculosis Infection in TNF-Deficient Mice. *J. Immunol.* **171**, 3110–3118 (2003).

73. Matty, M. A., Roca, F. J., Cronan, M. R. & Tobin, D. M. Adventures within the speckled band: heterogeneity, angiogenesis, and balanced inflammation in the tuberculous granuloma. *Immunol. Rev.* **264**, 276–287 (2015).

74. Tobin, D. M. *et al.* The lta4h Locus Modulates Susceptibility to Mycobacterial Infection in Zebrafish and Humans. *Cell* **140**, 717–730 (2010).

75. Tobin, D. M. *et al.* Host genotype-specific therapies can optimize the inflammatory response to mycobacterial infections. *Cell* **148**, 434–446 (2012).

76. Franchi, L., Eigenbrod, T. & Núñez, G. Cutting edge: TNF-alpha mediates

sensitization to ATP and silica via the NLRP3 inflammasome in the absence of microbial stimulation. *J. Immunol.* **183**, 792–796 (2009).

77. Bauernfeind, F., Niepmann, S., Knolle, P. A. & Hornung, V. Aging-Associated TNF Production Primes Inflammasome Activation and NLRP3-Related Metabolic Disturbances. *J. Immunol.* **197**, 2900–2908 (2016).

78. Jesus, A. A. & Goldbach-Mansky, R. IL-1 Blockade in Autoinflammatory Syndromes 1. doi:10.1146/annurev-med-061512-150641.

79. Sugawara, I., Yamada, H., Hua, S. & Mizuno, S. Role of interleukin (IL)-1 type 1 receptor in mycobacterial infection. *Microbiol. Immunol.* **45**, 743–750 (2001).

80. Di Paolo, N. C. *et al.* Interdependence between Interleukin-1 and Tumor Necrosis Factor Regulates TNF-Dependent Control of Mycobacterium tuberculosis Infection. *Immunity* **43**, 1125–1136 (2015).

81. Yamada, H., Mizumo, S., Horai, R., Iwakura, Y. & Sugawara, I. Protective role of interleukin-1 in mycobacterial infection in IL-1 α/β double-knockout mice. *Lab. Investig.* **80**, 759–767 (2000).

82. Mayer-Barber, K. D. *et al.* Innate and adaptive interferons suppress IL-1α and IL-1β production by distinct pulmonary myeloid subsets during Mycobacterium tuberculosis infection. *Immunity* **35**, 1023–1034 (2011).

83. Silvério, D., Gonçalves, R., Appelberg, R. & Saraiva, M. Advances on the Role and Applications of Interleukin-1 in Tuberculosis. *MBio* **12**, (2021).

84. Ji, D. X. *et al.* Type I interferon-driven susceptibility to Mycobacterium tuberculosis is mediated by IL-1Ra. *Nature Microbiology* vol. 4 2128–2135 (2019).

85. Dube, P. H., Revell, P. A., Chaplin, D. D., Lorenz, R. G. & Miller, V. L. A role for

IL-1 alpha in inducing pathologic inflammation during bacterial infection. *Proc. Natl. Acad. Sci. U. S. A.* **98**, 10880–5 (2001).

86. Jung, C. *et al.* Yersinia pseudotuberculosis disrupts intestinal barrier integrity through hematopoietic TLR-2 signaling. *J. Clin. Invest.* **122**, 2239–2251 (2012).

87. Dinarello, C. A. Overview of the IL-1 family in innate inflammation and acquired immunity. *Immunol. Rev.* **281**, 8–27 (2018).

88. Orzalli, M. H. *et al.* An Antiviral Branch of the IL-1 Signaling Pathway Restricts Immune-Evasive Virus Replication. *Mol. Cell* **71**, 825-840.e6 (2018).

89. Overcast, G. R. *et al.* IEC-intrinsic IL-1R signaling holds dual roles in regulating intestinal homeostasis and inflammation. *J. Exp. Med.* **220**, (2023).

90. Deyerle, K. L., Sims, J. E., Dower, S. K. & Bothwell, M. A. Pattern of IL-1 receptor gene expression suggests role in noninflammatory processes. *J. Immunol.* **149**, 1657–1665 (1992).

91. Al-Sadi, R. M. & Ma, T. Y. IL-1beta causes an increase in intestinal epithelial tight junction permeability. *J. Immunol.* **178**, 4641–4649 (2007).

92. Yan, S. R., Joseph, R. R., Wang, J. & Stadnyk, A. W. Differential Pattern of Inflammatory Molecule Regulation in Intestinal Epithelial Cells Stimulated with IL-1. *J. Immunol.* **177**, 5604–5611 (2006).

93. Satpathy, A. T. *et al.* Notch2-dependent classical dendritic cells orchestrate intestinal immunity to attaching-and-effacing bacterial pathogens. *Nat. Immunol.* **14**, 937–948 (2013).

94. Pfeffer, K. *et al.* Mice deficient for the 55 kd tumor necrosis factor receptor are resistant to endotoxic shock, yet succumb to L. monocytogenes infection. *Cell* **73**,

457–467 (1993).

95. Berger, S. B. *et al.* Cutting Edge: RIP1 kinase activity is dispensable for normal development but is a key regulator of inflammation in SHARPIN-deficient mice. *J. Immunol.* **192**, 5476–5480 (2014).

96. Glaccum, M. B. *et al.* Phenotypic and functional characterization of mice that lack the type I receptor for IL-1. *J. Immunol.* **159**, 3364–3371 (1997).

97. Horai, R. *et al.* Production of Mice Deficient in Genes for Interleukin (IL)-1α, IL-1β, IL-1α/β, and IL-1 Receptor Antagonist Shows that IL-1β Is Crucial in Turpentine-induced Fever Development and Glucocorticoid Secretion. *J. Exp. Med.* **187**, 1463–1475 (1998).

98. Simonet, M. & Falkow, S. Invasin expression in Yersinia pseudotuberculosis. *Infect. Immun.* **60**, 4414–4417 (1992).

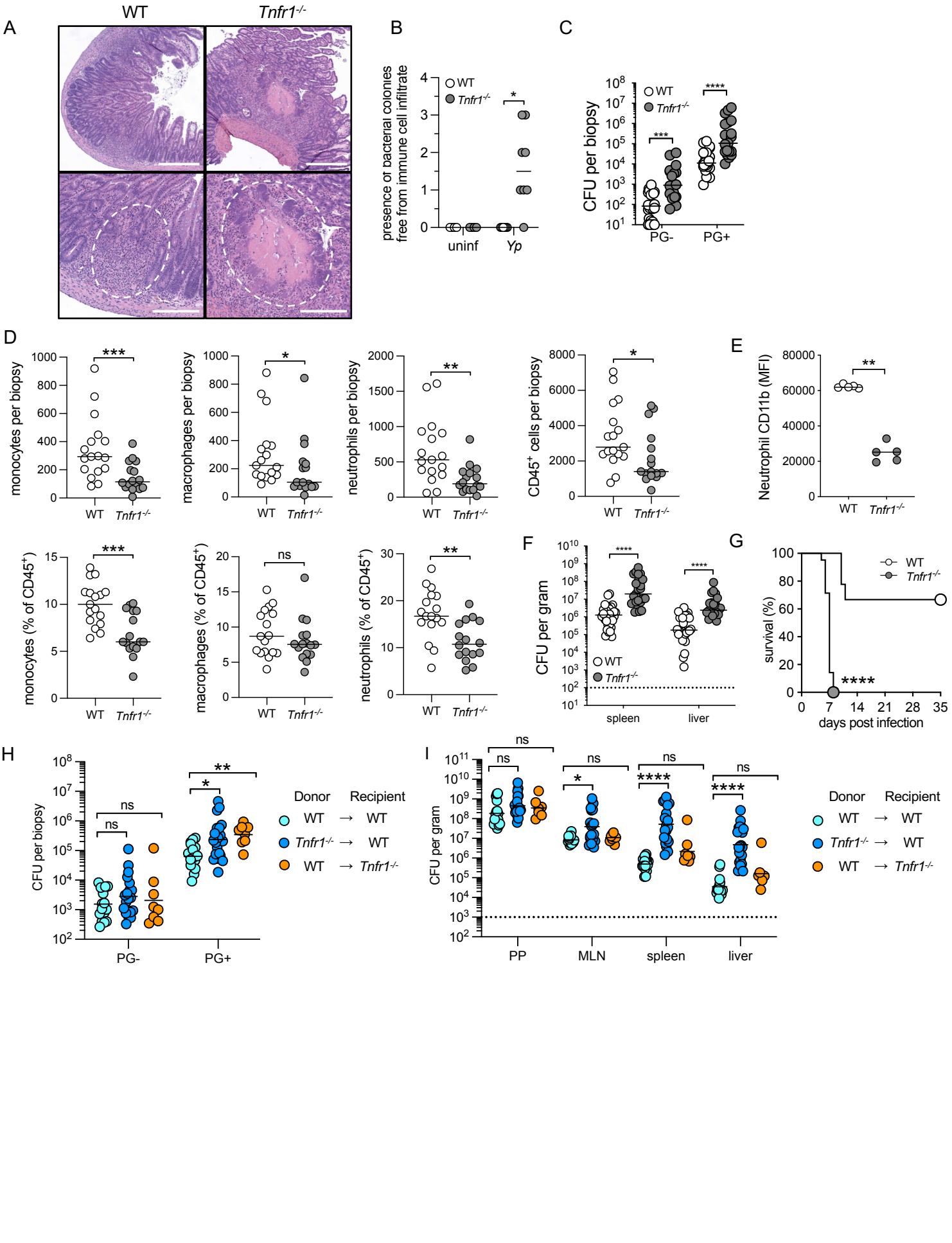
A
WT
Tnfr1-/-
B
presence of bacterial colonies free from immune cell infiltrate
WT
Tnfr1-/-
uninf
Yp
C
CFU per biopsy
PG-
PG+
D
monocytes per biopsy
macrophages per biopsy
neutrophils per biopsy
CD45+ cells per biopsy
monocytes (% of CD45+)
macrophages (% of CD45+)
neutrophils (% of CD45+)
ns
E
Neutrophil CD11b (MFI)
F
CFU per gram
spleen
liver
G
survival (%)
days post infection
H
CFU per biopsy
Donor
Recipient
WT → WT
Tnfr1-/- → WT
WT → Tnfr1-/-
I
CFU per gram
PP
MLN
spleen
liver

Figure 1. TNFR1 is required for organized pyogranuloma formation and restriction of *Yersinia*

(**A**) H&E-stained paraffin-embedded longitudinal small intestinal sections from *Yp*-infected mice at day 5 post-infection. Dashed line highlights pyogranuloma (left) or necrosuppurative lesion (right). Images representative of two experiments. Scale bars = 500 μm (top) and 200 μm (bottom).

(**B**) Histopathological scores of small intestinal tissue from uninfected or *Yp*-infected mice at day 5 post-infection. Each mouse was scored between 0-4 (healthy-severe) for indicated sign of pathology. Each circle represents one mouse. Lines represent median. Pooled data from two experiments.

(**C**) Bacterial burdens in small-intestinal PG- and PG+ tissue isolated day 5 post-infection. Each circle represents the mean CFU of 3-5 pooled punch biopsies from one mouse. Lines represent geometric mean. Pooled data from three independent experiments.

(**D**) Total numbers and frequencies of $CD45^+$ cells, monocytes, macrophages, and neutrophils in uninfected, PG-, and PG+ small intestinal tissue isolated 5 days post-infection. Each circle represents the mean of 3-10 pooled punch biopsies from one mouse. Lines represent median. Pooled data from three independent experiments.

(**E**) Mean fluorescence intensity (MFI) of CD11b expression on neutrophils in PG+ tissue at day 5 post-infection. Each circle represents the mean of 3-10 pooled punch biopsies from one mouse. Lines represent median. Data representative of three independent experiments.

(**F**) Bacterial burdens in indicated organs at day 5 post-infection. Each circle represents one mouse. Lines represent geometric mean. Pooled data from four independent experiments.

(**G**) Survival of infected WT (n=9) and *Tnfr1*$^{-/-}$ (n=21) mice. Pooled data from two independent experiments.

(**H**) Bacterial burdens in small-intestinal PG- and PG+ tissue at day 5 post-infection of indicated chimeric mice. Each circle represents the mean *Yp*-CFU of 3-5 pooled punch biopsies from one mouse. Lines represent geometric mean. Pooled data from two independent experiments.

(**I**) Bacterial burdens in indicated organs at day 5 post-infection of indicated chimeric mice. Each circle represents one mouse. Lines represent geometric mean. Pooled data from two independent experiments.

Statistical analysis by (B, C, D, E, F) Mann-Whitney U test (G) Mantel-Cox test (H, I) Kruskal-Wallis test with Dunn's multiple comparisons correction. *p<0.05, **p<0.01, ***p<0.001, ****p<0.0001, ns = not significant.

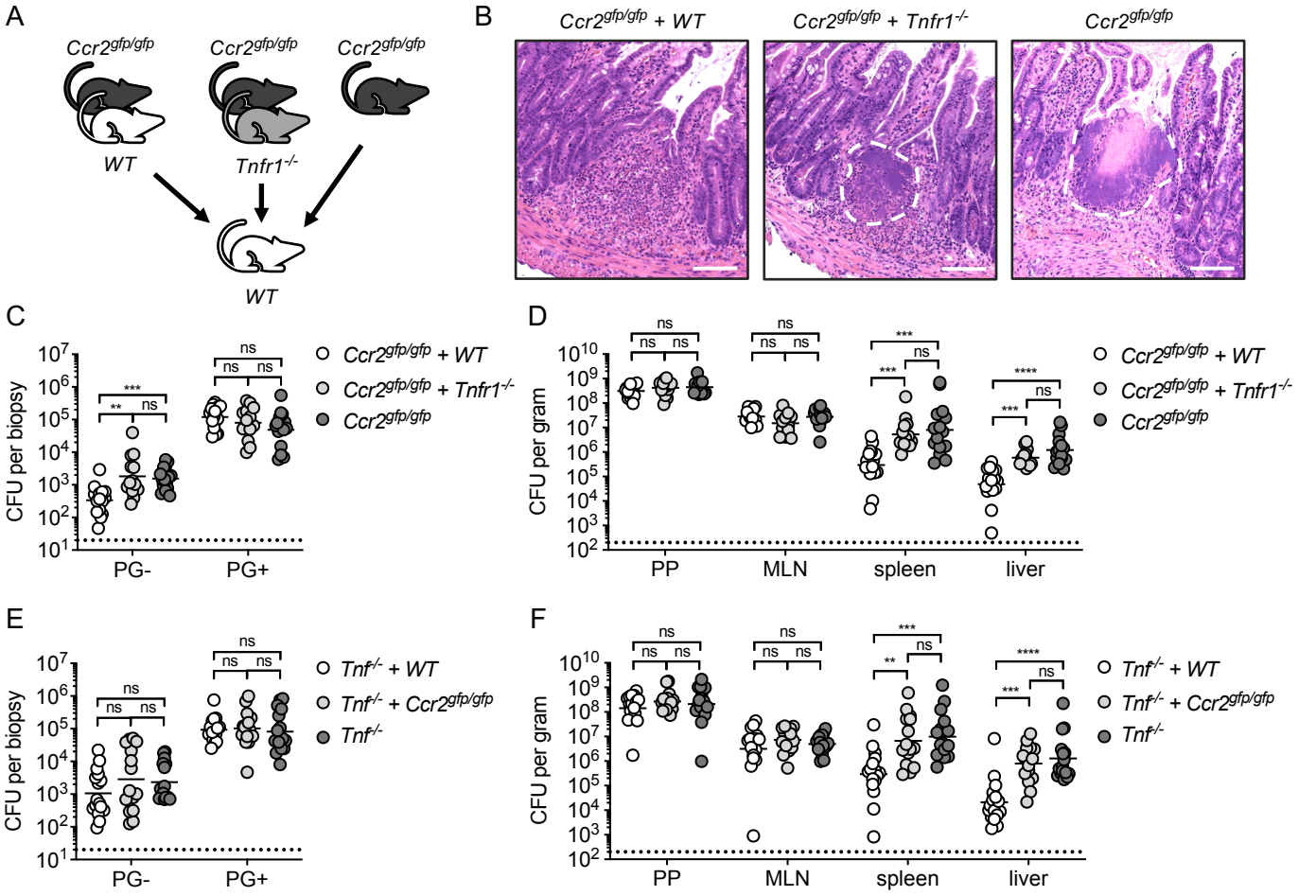

Figure 2. Autocrine TNF signaling in monocytes is required for control of *Yersinia*

(**A**) Schematic of mixed bone marrow chimeras.

(**B**) H&E-stained paraffin-embedded transverse small-intestinal sections from chimeric WT mice reconstituted with *Ccr2*$^{gfp/gfp}$ + *WT* (left), *Ccr2*$^{gfp/gfp}$ + *Tnfr1*$^{-/-}$ (middle), or *Ccr2*$^{gfp/gfp}$ (right) bone marrow, at day 5 post-infection. Dotted lines highlight lesions. Scale bars = 100 µm. Images representative of two independent experiments.

(**C**) Bacterial burdens in small-intestinal PG- and PG+ tissue of chimeric WT mice reconstituted with either *Ccr2*$^{gfp/gfp}$ + *WT* (white), *Ccr2*$^{gfp/gfp}$ + *Tnfr1*$^{-/-}$ (light gray), or *Ccr2*$^{gfp/gfp}$ (dark gray) at day 5 post *Yp*-infection. Each symbol represents one mouse. Lines represent geometric mean. Pooled data from two independent experiments.

(**D**) Bacterial burdens in indicated organs at day 5 post-infection. Each circle represents one mouse. Lines represent geometric mean. Pooled data from two independent experiments.

(**E**) Bacterial burdens in small-intestinal PG- and PG+ tissue of chimeric WT mice reconstituted with either *Tnf*$^{-/-}$ + *WT* (white), *Tnf*$^{-/-}$ + *Ccr2*$^{gfp/gfp}$ (light gray), or *Tnf*$^{-/-}$ (dark gray) at day 5 post *Yp*-infection. Each symbol represents one mouse. Lines represent geometric mean. Pooled data from three independent experiments.

(**F**) Bacterial burdens in indicated organs at day 5 post-infection. Each circle represents one mouse. Lines represent geometric mean. Pooled data from three independent experiments.

Statistical analysis by Kruskal-Wallis test with Dunn's multiple comparisons correction. *p<0.05, **p<0.01, ***p<0.001, ****p<0.0001, ns = not significant.

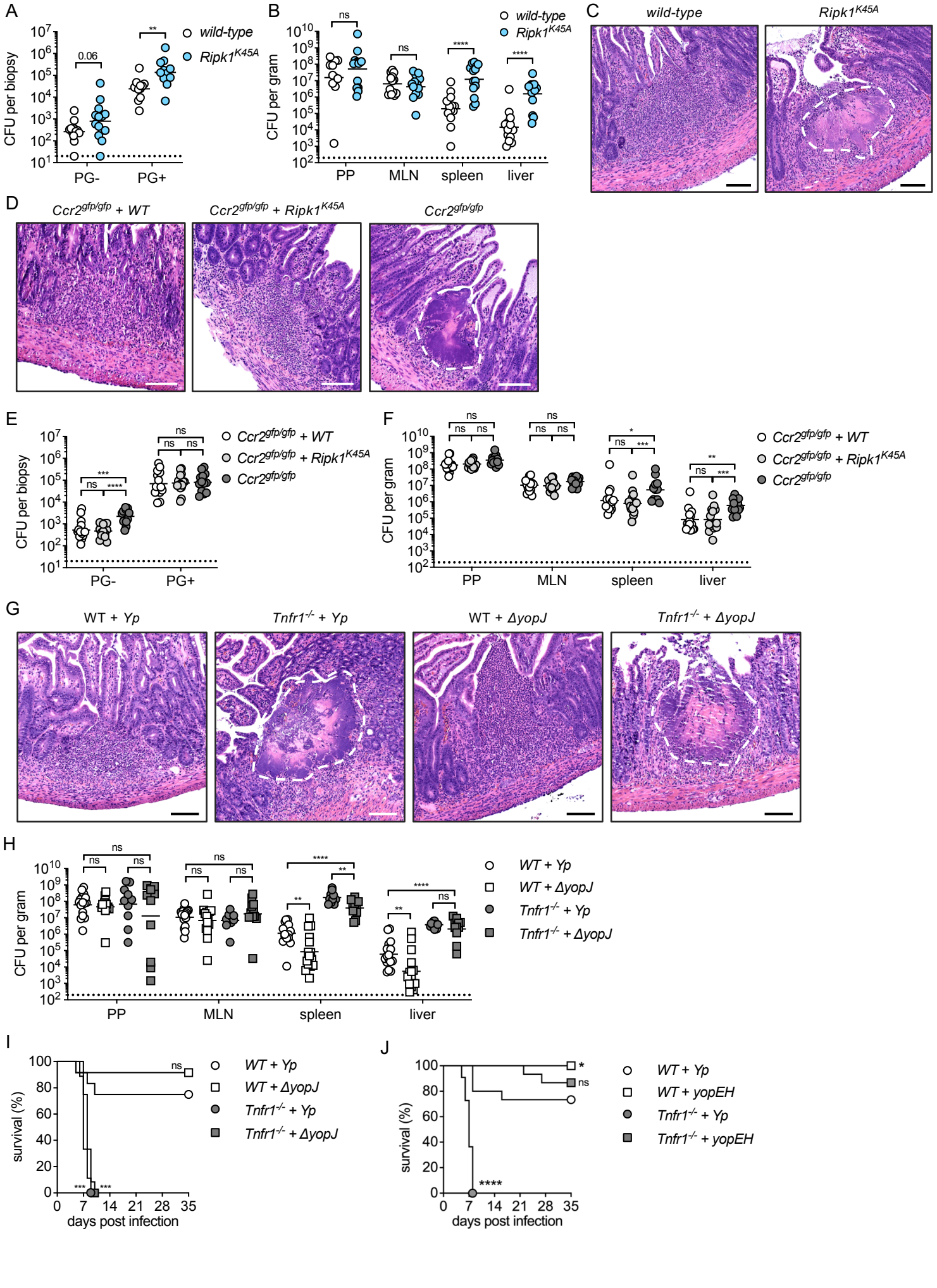
A
CFU per biopsy
wild-type
Ripk1K45A
0.06
**
PG-
PG+
B
CFU per gram
ns
****
PP
MLN
spleen
liver
C
wild-type
Ripk1K45A
D
Ccr2gfp/gfp + WT
Ccr2gfp/gfp + Ripk1K45A
Ccr2gfp/gfp
E
CFU per biopsy
Ccr2gfp/gfp + WT
Ccr2gfp/gfp + Ripk1K45A
Ccr2gfp/gfp
***
PG-
PG+
F
CFU per gram
*
**
***
PP
MLN
spleen
liver
G
WT + Yp
Tnfr1-/- + Yp
WT + ΔyopJ
Tnfr1-/- + ΔyopJ
H
CFU per gram
WT + Yp
WT + ΔyopJ
Tnfr1-/- + Yp
Tnfr1-/- + ΔyopJ
PP
MLN
spleen
liver
I
survival (%)
days post infection
WT + Yp
WT + ΔyopJ
Tnfr1-/- + Yp
Tnfr1-/- + ΔyopJ
J
survival (%)
days post infection
WT + Yp
WT + yopEH
Tnfr1-/- + Yp
Tnfr1-/- + yopEH

Figure 3. TNFR1 signaling in monocytes controls *Yp* independently of RIPK1 kinase-induced cell death

(**A**) Bacterial burdens in small-intestinal PG- and PG+ tissue of WT (white) and *Ripk1*^{K45A} (blue) mice at day 5 post *Yp*-infection. Each symbol represents one mouse. Lines represent geometric mean. Pooled data from two independent experiments.

(**B**) Bacterial burdens in indicated organs at day 5 post-infection. Each circle represents one mouse. Lines represent geometric mean. Pooled data from two independent experiments.

(**C**) H&E-stained paraffin-embedded longitudinal small-intestinal sections from *WT* (left) and *Ripk1*^{K45A} (right) mice at day 5 post *Yp*-infection with dotted line highlighting lesion. Scale bars = 100 µm. Representative images of two independent experiments.

(**D**) H&E-stained paraffin-embedded transverse small-intestinal sections from chimeric WT mice reconstituted with either *Ccr2*$^{gfp/gfp}$ + *WT* (left), *Ccr2*$^{gfp/gfp}$ + *Ripk1*^{K45A} (middle), or *Ccr2*$^{gfp/gfp}$ (right) bone marrow, at day 5 post *Yp*-infection with dotted line highlighting lesion. Scale bars = 100 µm. Representative images of two independent experiments.

(**E**) Bacterial burdens in small-intestinal PG- and PG+ tissue of chimeric WT mice reconstituted with either *Ccr2*$^{gfp/gfp}$ + *WT* (white), *Ccr2*$^{gfp/gfp}$ + *Ripk1*^{K45A} (light gray), or *Ccr2*$^{gfp/gfp}$ (dark gray) at day 5 post *Yp*-infection. Each symbol represents one mouse. Lines represent geometric mean. Pooled data from two independent experiments.

(**F**) Bacterial burdens in indicated organs at day 5 post-infection. Each circle represents one mouse. Lines represent geometric mean. Pooled data from two independent experiments.

(**G**) H&E-stained paraffin-embedded longitudinal small-intestinal sections from *wild-type* and *Tnfr1*$^{-/-}$ mice infected with either *WT* or *ΔyopJ Yp* at day 5 post-infection. Scale bars = 100 µm. Representative images of three independent experiments.

(**H**) Bacterial burdens in indicated organs at day 5 post-infection. Each circle represents one mouse. Lines represent geometric mean. Pooled data from four independent experiments.

(**I**) Survival of wild-type (white) and *Tnfr1*$^{-/-}$ (gray) mice infected with WT (circles) or *ΔyopJ* (squares) *Yp*. N = 9-12 mice per group. Pooled data from two independent experiments.

(**J**) Survival of WT (white) or *Tnfr1*$^{-/-}$ (gray) mice infected with WT (circles) or *yopEH* (squares) *Yp*. n = 11-15 mice per group. Pooled data from two independent experiments.

Statistical analysis by Mann-Whitney U test (A, B), Kruskal-Wallis test with Dunn's multiple comparisons correction (E, F, H), or Mantel-Cox test (I, J). *p<0.05, **p<0.01, ***p<0.001, ****p<0.0001, ns = not significant.

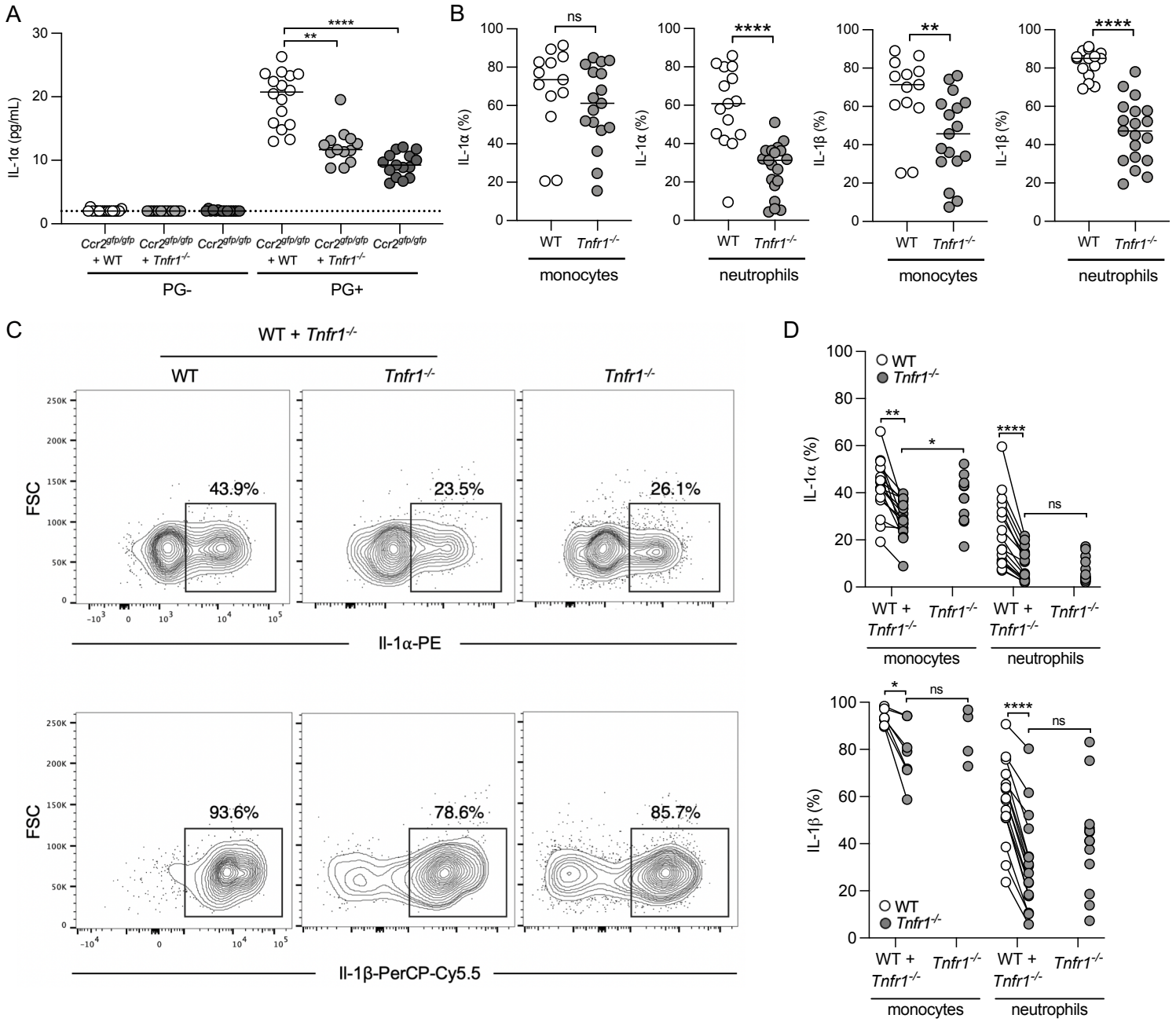

Figure 4. Cell-intrinsic TNFR1 signaling is required for maximal IL-1 production within intestinal pyogranulomas during *Yersinia* infection

(**A**) Cytokine levels were measured by cytometric bead array in tissue punch biopsy homogenates isolated 5 days post-infection of chimeric WT mice reconstituted with indicated donor cells. Lines represent median. Pooled data from two independent experiments.

(**B**) Intracellular cytokine levels in monocytes and neutrophils isolated from small intestinal PG+ tissue 5 days post-infection. Each circle represents the mean of 3-10 pooled punch biopsies from one mouse. Lines represent median. Pooled data from three independent experiments.

(**C**) Flow cytometry plots of intracellular IL-1 in monocytes ($CD64^+$ $Ly\text{-}6C^{hi}$) from small intestinal PG+ tissue at day 5 post-infection. Plots representative of two independent experiments.

(**D**) Aggregate datasets from (C) for intracellular IL-1 staining in monocytes and neutrophils in small intestinal PG+ tissue at day 5 post-infection. Each circle represents the mean of 3-10 pooled punch biopsies from one mouse. Lines connect congenic cell populations within individual mice. Pooled data from two independent experiments.

Statistical analysis by (A) Kruskal-Wallis test with Dunn's multiple comparisons correction (B) Mann-Whitney U test (D) congenic cells within mice: Wilcoxon test; across groups: Mann-Whitney U test. *p<0.05, **p<0.01, ***p<0.001, ****p<0.0001, ns = not significant.

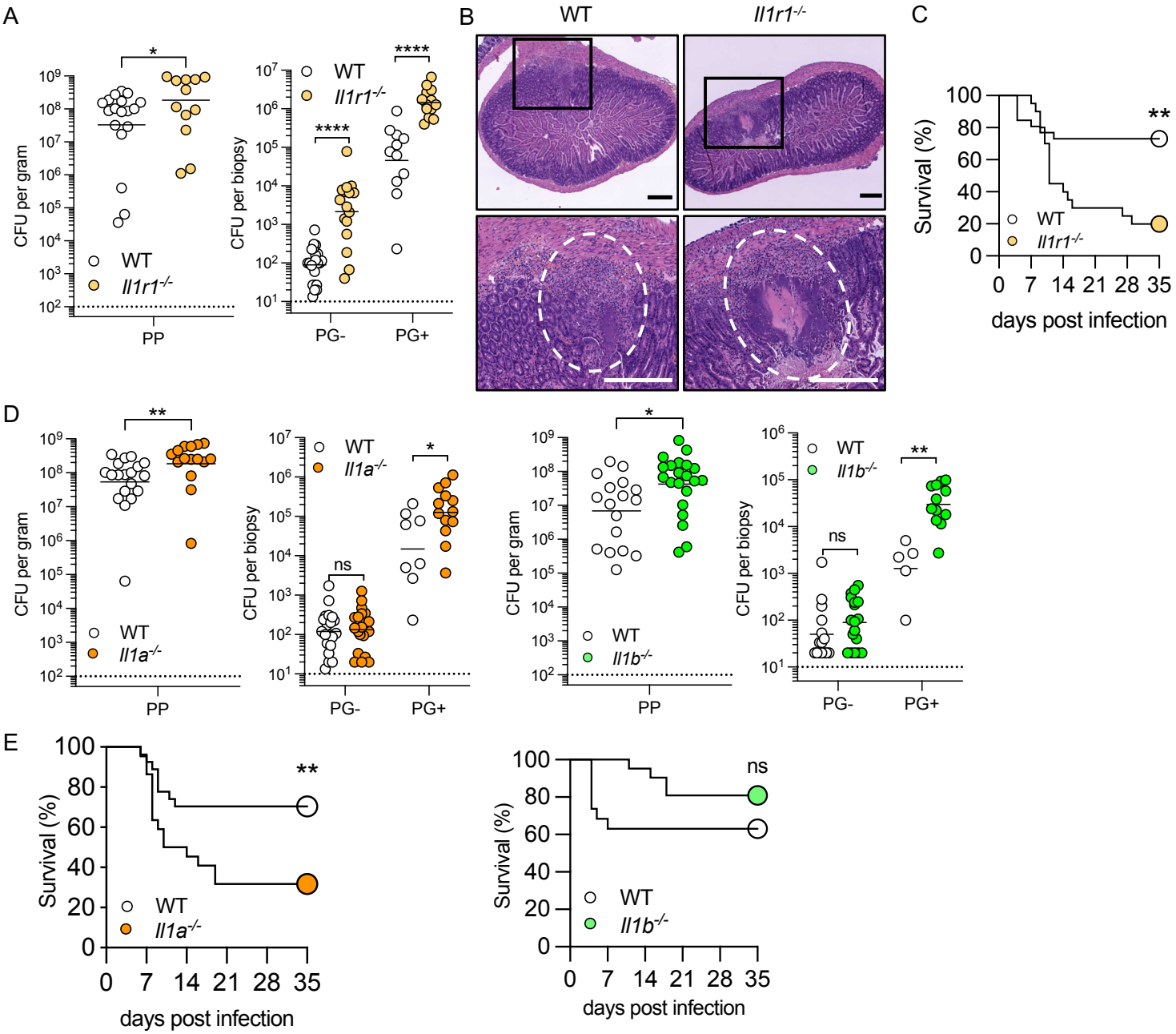

Figure 5. IL-1 signaling is required for organized pyogranuloma formation and intestinal control of *Yersinia*

(A) Bacterial burdens in small-intestinal Peyer's patches (PP), PG-, and PG+ tissues isolated 5 days post-infection. For PP each circle represents one mouse. For PG- and PG+ each circle represents the mean of 3-5 pooled punch biopsies from one mouse. Lines represent geometric mean. Pooled data from three independent experiments.

(B) H&E-stained paraffin-embedded longitudinal small intestinal sections from *Yp*-infected mice at day 5 post-infection. Representative images of one experiment. Scale bars = 250 μm.

(C) Survival of infected WT (n=26) and *Il1r1*$^{-/-}$ (n=20) mice. Pooled data from two independent experiments

(D). Bacterial burdens in small-intestinal PP, PG-, and PG+ tissues at day 5 post-infection of indicated genotypes. For PP each circle represents one mouse. For PG- and PG+ each circle represents the mean of 3-5 pooled punch biopsies from one mouse. Lines represent geometric mean. Pooled data from three independent experiments.

(E). Survival of infected WT (n=27, n=19), *Il1a*$^{-/-}$ (n=22) and *Il1b*$^{-/-}$ (n=21) mice. Pooled data from three and two independent experiments. Statistical analysis by (A, D) Mann-Whitney U test (C, E) Manel-Cox test. *p<0.05, **p<0.01, ****p<0.0001, ns = not significant.

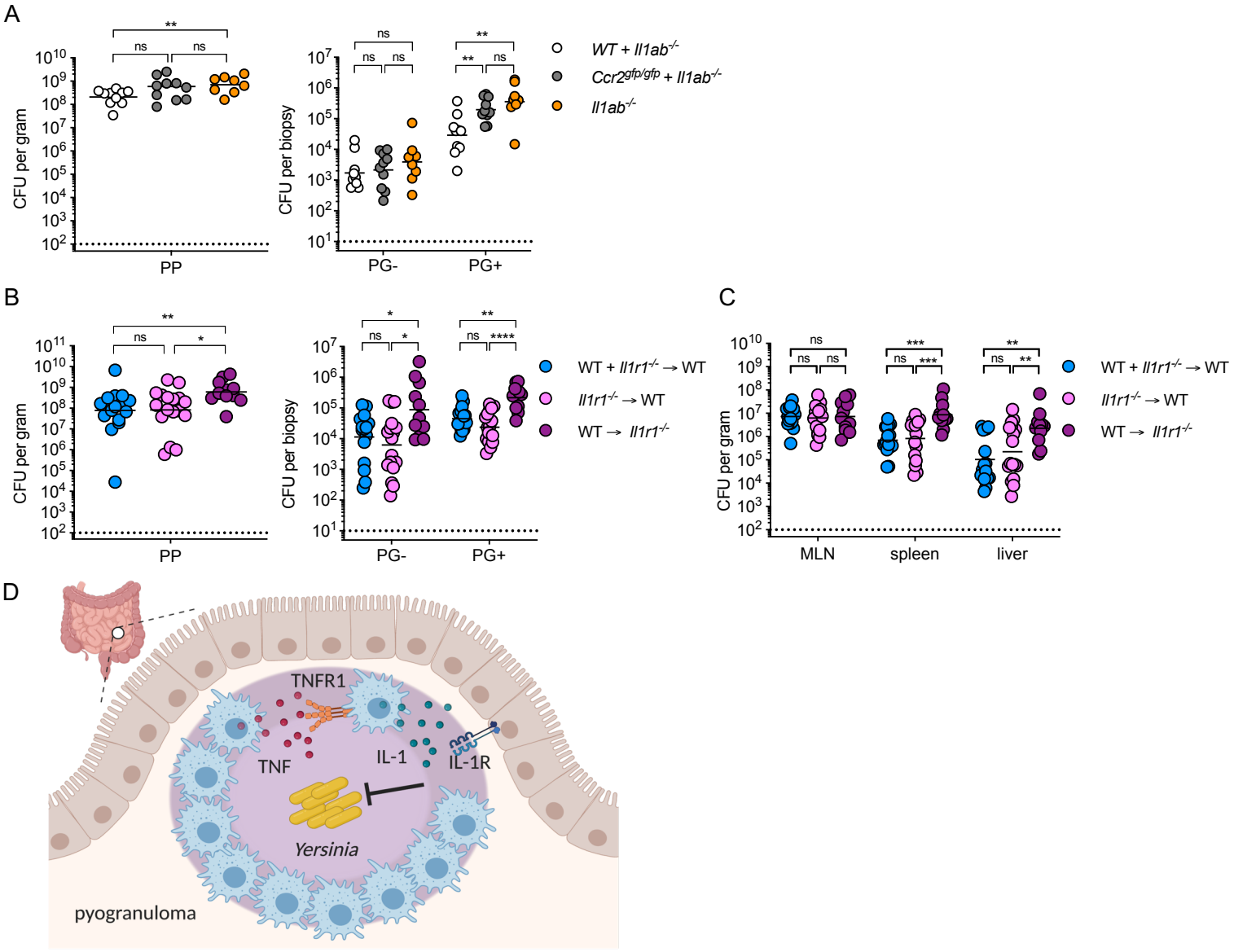

Figure 6. Monocyte-derived IL-1 signals to nonhematopoietic cells to restrict *Yersinia* infection in intestinal pyogranulomas

(A) Bacterial burdens in small-intestinal Peyer's patches (PP), PG-, and PG+ tissues at day 5 post-infection of indicated chimeric mice. For PP each circle represents one mouse. For PG- and PG+ each circle represents the mean of 3-5 pooled punch biopsies from one mouse. Lines represent geometric mean. Data pooled from two independent experiments.

(C) Bacterial burdens in small-intestinal Peyer's patches (PP), PG-, and PG+ tissues isolated 5 days post-infection of indicated chimeric mice. For PP each circle represents one mouse. For PG- and PG+ each circle represents the mean of 3-5 pooled punch biopsies from one mouse. Lines represent geometric mean. Pooled data from three independent experiments.

(C) Bacterial burdens in indicated organs at day 5 post-infection of indicated chimeric mouse. Each circle represents one mouse. Lines represent geometric mean. Data pooled from three independent experiments.

All statistical analysis by Kruskal-Wallis test with Dunn's multiple comparisons correction. *p<0.05, **p<0.01, ***p<0.001, ns = not significant.

(D) Model of TNF-IL-1 circuit mediated by monocyte and stromal compartment to promote *Yp* restriction in intestinal pyogranulomas.